EPA-600/1-79-025
August 1979

ABSORPTION CHARACTERISTICS OF PROLATE SPHEROIDAL MODEL OF MAN AND ANIMALS AT AND NEAR RESONANCE FREQUENCY

by

Vijai K. Tripathi and Hyuckjae Lee
The Department of Electrical and Computer Engineering
Oregon State University
Corvallis, Oregon 97331

R-804697-01-1

Project Officer

Claude M. Weil
Health Effects Research Laboratory
Research Triangle Park, North Carolina 27711

Health Effects Research Laboratory
Office of Research and Development
U.S. Environmental Protection Agency
Research Triangle Park, North Carolina 27711

DISCLAIMER

This report has been reviewed by the Health Effects Research Laboratory, U.S. Environmental Protection Agency, and approved for publication. Approval does not signify that the contents necessarily reflect the views and policies of the U.S. Environmental Protection Agency, nor does mention of trade names or commercial products constitute endorsement or recommendation for use.

FOREWORD

The Health Effects Research Laboratory (HERL), a part of EPA's Office of Research and Development, is responsible for performing research into the health impacts on mankind of many environmental pollutants, as well as undesirable physical factors within the environment. One of the latter factors with which HERL concerns itself is nonionizing electromagnetic (radiofrequency and microwave) radiation. The basic objective of EPA's research program into the health implications of nonionizing radiation is to develop scientific criteria upon which the Agency can develop an environmental exposure standard for radiofrequency (RF) radiation.

Much of the in-house research performed to date at HERL's Research Triangle Park, NC facility has involved chronic exposures of experimental animals to radiation of various wavelength within the RF spectrum. In these experiments, animals have generally been assessed in a number of different areas such as development, teratology, immunology, hematology, behavior, neurochemistry, etc., in order to determine whether any possible adverse effects exist. Accurate characterization of these experiments requires a knowledge of the RF energy (or dose) which the animal is absorbing as well as the internal energy distribution. Furthermore, there is an obvious need to try to extrapolate animal findings to humans, a problem that is particularly complex and difficult for nonionizing radiation. The data needed for such extrapolations cannot be readily derived by experimental means.

For these reasons, many investigators active in this field of research have made use of simplified mathematical models which have yielded much data that is useful for predicting approximately the energy absorption in both animals and man under various conditions of RF irradiation. Because of their obvious similarity to the external shape of both man and experimental animals, models of prolate spheroidal and ellipsoidal shape have been investigated by several workers. These are composed of dissipative (lossy) dielectric and the exposure is generally to a plane wave. Previous workers had succeeded in obtaining a quasi-static solution valid in the low frequency region where incident wavelength is greater than the physical dimensions of the prolate spheroid and ellipsoidal model. However, no solutions were available in the resonant and near-resonant region where the incident wavelength is comparable to the object dimensions. This region is of considerable importance because maximum coupling of electromagnetic energy into the exposed object occurs in the resonant region. Solutions to the problem involving a prolate spheroid of dimensions similar to that of man in the resonant frequency region would provide realistic estimates of the maximum thermal burden which man would likely be subjected to under these worst-case conditions. Such data have obvious applicability to the setting of RF protection standards.

Consequently, a study was sponsored through a research grant to Oregon State University, whose purpose was to investigate possible solutions to the electromagnetic problem involving the lossy prolate spheroid model in the resonant region. All of the existing techniques were to be reviewed and the limitations and restrictions on the applicability of such techniques to this particular problem were to be detailed. In particular, the feasibility of applying the separation of variables technique to this problem was to be examined since this technique does yield highly accurate solutions for the closely related problem involving lossy sphere models in the resonant region. This report details the results of this study. In attempting to summarize the conclusions of the report, it may be stated that accurate solutions are presently available in the resonant region for prolate spheroid models of low to medium eccentricity applicable to experimental animals, but that no solutions are as yet available in the resonant region for highly eccentric (i.e., elongated) models similar to man owing to mathematical difficulties encountered in the solution of this problem. Further work is needed to overcome these difficulties before a solution to this important problem becomes available.

Readers' comments on any aspect of this report are solicited by the HERL project officer.

F.G. Hueter, Ph.D., Director
Health Effects Research Laboratory

ABSTRACT

This report deals with the evaluation of the absorption characteristics of prolate spheroidal models of man and animals consisting of homogeneous biological tissues irradiated with plane waves at an arbitrary angle of incidence at and near the resonance frequency. Stevenson's series expansion method in the third approximation and the extended boundary condition method are presented in detail since they were found to be most amenable to the solution of the problem.

It is shown that Stevenson's method in the third approximation can be applied to solve for the absorption cross sections of prolate spheroidal and ellipsoidal models at lower frequencies. The method is quite general as compared to other known long wavelength analysis methods which are applicable to high conductivity models at nose-on and broadside incidences only. The general formulation presented in the report can be applied to an arbitrary angle of incidence and leads to an improvement in frequency range of validity and accuracy as compared to the first order solutions. Numerical results for prolate spheroidal models are presented and are compared with known results for first order solutions and the general time-dependent solutions obtained by the extended boundary condition method.

It is also shown that the problem of the absorption by lossy prolate spheroidal objects can be formulated in general by utilizing other methods such as the separation of variables and the point matching techniques. However, the extended boundary condition method (EBCM) was found to be implementable for realistic models over a wide range of frequencies. Even though the theory of EBCM is well known, this report emphasizes the application of the method, and contains some modifications for improving the accuracy and efficiency of the computations. Numerical results obtained by utilizing this method are also presented.

This report was submitted in fulfillment of Grant No. R-804697-01-1 by Oregon State University under the sponsorship of U.S. Environmental Protection Agency. This report covers a period of September 15, 1976 to March 15, 1978.

CONTENTS

Foreward iii
Abstract v

1. Introduction 1
2. Theoretical Formulation 3

2.1. Statement of the Problem 3
2.2. Stevenson's Method in the Third Approximation 5

2.2.1. Theoretical Formulation 6
2.2.2. Comparison with Long Wavelength Results 9
2.2.3. Prolate Spheroidal Model 10

2.3. Point Matching Method 11
2.4. Separation of Variables Method 11
2.5. Extended Boundary Condition Method 12

3. Numerical Results 13
4. Conclusions and Suggestions for Further Study 20

4.1. Conclusions 20
4.2. Suggestions for Further Work 21

References 22
Appendices

A. Scattering Coefficients 25
B. Prolate Spheroidal Model - Expressions for Coefficients 28

Case 1 - Broadside Incidence - Electric Field Along the Major Axis 28
Case 2 - Broadside Incidence - Magnetic Field Along the Major Axis 29
Case 3 - Nose-On Incidence 29

C. Extended Boundary Condition Method 31

C-1. Theoretical Formulation 31
C-2. Extended Boundary Condition Applied to the Surface 36
C-3. Application to Spheroidal Problem 39

D. Description of Computer Program for EBCM 43

D-1. Introduction 43
D-2. Glossary of Subroutines 43
D-3. Computation of Special Functions 44
D-4. Computation of Geometrical Factors 46
D-5. Computation of Scattering, Absorption and Extinction Characteristics 46
D-6. Integration Schemes 47
D-7. Description of Variables Used in the Program 47
D-8. Inputs to the Program 49
D-9. Outline of the General Flow of the Program 50
D-10. Program Listings 51

SECTION 1

INTRODUCTION

A great deal of work has been done in recent years on the biological effects of electromagnetic radiation. One important aspect of this work involves the determination of internal distribution of power absorbed at any specified biological tissue in the body and the total power absorbed by the body subjected to electromagnetic radiation. Power is absorbed by the tissues as a function of body shape, tissue properties, frequency and incident radiation.

As a first step in this direction, uniform and layered tissue spherical models have been analysed by a number of workers. Most of the early work had been confined to a spherical model due to the relative ease of analysis. Early work on the uniform sphere model has been done by Anne et al. [1], Shapiro et al. [2], Kritikos and Schwan [3] and Johnson and Guy [4]. The analyses of multilayered tissue model have been conducted by Joines and Spiegel [5] and Weil [6]. These analyses are applicable to all frequency ranges. Based on these models, in which energy deposition has been confirmed for the uniform sphere case by thermographic camera photographs of irradiated phantom models [4,7], it is expected that the power deposition pattern in man and animals varies greatly with the properties of incident radiation including frequency, body configuration and orientation. This leads to a need for analytical tools to describe power absorption patterns in more realistic models of man and animals as a function of incident radiation. A model more realistic than a sphere for the human body and many animal bodies is the prolate spheroid.

A low frequency analysis of a uniform ellipsoid and prolate spheroid model has been conducted by Durney, Johnson and Massoudi [8-11] using Stevenson's method [12,13] as given in Van Bladel [14]. Their results, particularly the effect of object orientation with respect to the incident plane wave vectors, indicate a significant difference from results for the spherical models at low frequencies and underline the need for a solution of the prolate spheroidal model problem at higher frequencies at and near the resonance frequencies. At higher frequencies, as characterized loosely by $0.3 \leq kb \leq 300$, where b is the largest semi-axis, the solution cannot be accurately determined using this method unless higher order (third and higher) solutions are included. Several other known techniques have also been tried recently by these authors and others at the higher frequencies with varying degrees of success . These include the point matching technique [15,16], the spheroidal function expansion method [17] and the extended boundary condition method [18,19]. At higher frequencies when skin-surface heating effects predominate, $kb \gg 1$, and the

so-called slab model, consisting of planar layers of skin, fat and tissue layers has been used to evaluate the electromagnetic power absorption [20,21].

The gap of information regarding the analysis and numerical results for electromagnetic power absorption in prolate spheroidal model at and near the resonance frequency needs to be filled since at resonance the absorption efficiency is greatest. These results are essential in order that researchers can obtain tissue absorbed power estimates in terms of incident electromagnetic radiation parameters in order to establish a sound electromagnetic safety standard over this important frequency band.

The primary objectives of this research program were to evaluate the absorption characteristics of the prolate spheroidal model of man and animals consisting of homogeneous tissue characterized by known values of $\varepsilon(\omega)$, $\sigma(\omega)$ and μ_0 at and near the resonance frequency when radiated with electromagnetic waves. The electromagnetic radiation is in the form of a plane wave propagating in an arbitrary direction polarized either in the plane of the wave vector and the major axis of the spheroid or normal to it.

A comprehensive investigation of several techniques was conducted in an attempt to arrive at the most convenient methods to solve for the absorption characteristics. These include:

- Stevenson's Method
- Separation of Variables Method in Prolate Spheroidal Coordinates
- Point Matching Technique
- Extended Boundary Condition Method (EBCM).

Even though the problem of electromagnetic scattering and absorption by lossy prolate spheroidal objects can be formulated by utilizing all of these methods, Stevenson's method in the third approximation and the EBCM were found to be the most efficient from a computational point of view. In addition, these methods were most successful in evaluating the absorption characteristics of realistic prolate spheroidal models within their respective range of validity. For these reasons these two methods and the results obtained by utilizing them have been emphasized in this report. Section 2 deals with the theoretical formulation of the problem with a particular emphasis on Stevenson's method in the third approximation as well as the EBCM. The numerical results obtained by utilizing these methods are presented in Section 3. A summary of results and suggestions for further work are presented in Section 4.

SECTION 2

THEORETICAL FORMULATION

2-1. STATEMENT OF THE PROBLEM

The prolate spheroid model is shown in Figure 1. The object is assumed to be homogeneous having conductivity σ, dielectric constant $\varepsilon = \varepsilon_o \varepsilon_r$ and permeability μ_o. The incident radiation is assumed to be a plane wave polarized in an arbitrary direction propagating along $\hat{a}_k$. Note that other wave fronts may be constructed by a super position of plane waves. Then the electric field of both regions (inside and outside the object) are a solution of the Helmholz wave equation as given by:

$$\nabla^2 \vec{E} + k^2 \vec{E} = 0 \tag{1}$$

for harmonically oscillating fields ($e^{j\omega t}$ variation), where

$$k^2 = k_o^2 = \omega^2 \mu_o \varepsilon_o, \text{ outside} \tag{2}$$

and

$$k^2 = k_1^2 = \omega^2 \mu_o \varepsilon + j\omega\mu_o \sigma \text{ inside the spheroid.} \tag{3}$$

The boundary conditions which the solution must satisfy at the interface are:

$$\hat{n} \times (\vec{E}_{ext} - \vec{E}_{int}) = 0 \tag{4}$$

and

$$\hat{n} \cdot [\varepsilon_o \vec{E}_{ext} - (\varepsilon - \frac{\sigma}{j\omega}) \vec{E}_{int}] = 0 \tag{5}$$

where, $\vec{E}_{ext}$, the external field is the sum of incident and scattered fields and E_{int} is the internal field in the spheroid: ε and σ are known constants [4].

Given an incident radiation which is assumed to be a plane wave, $\vec{E}_{int}$, can be determined by solving the equations (1) - (5) given above.

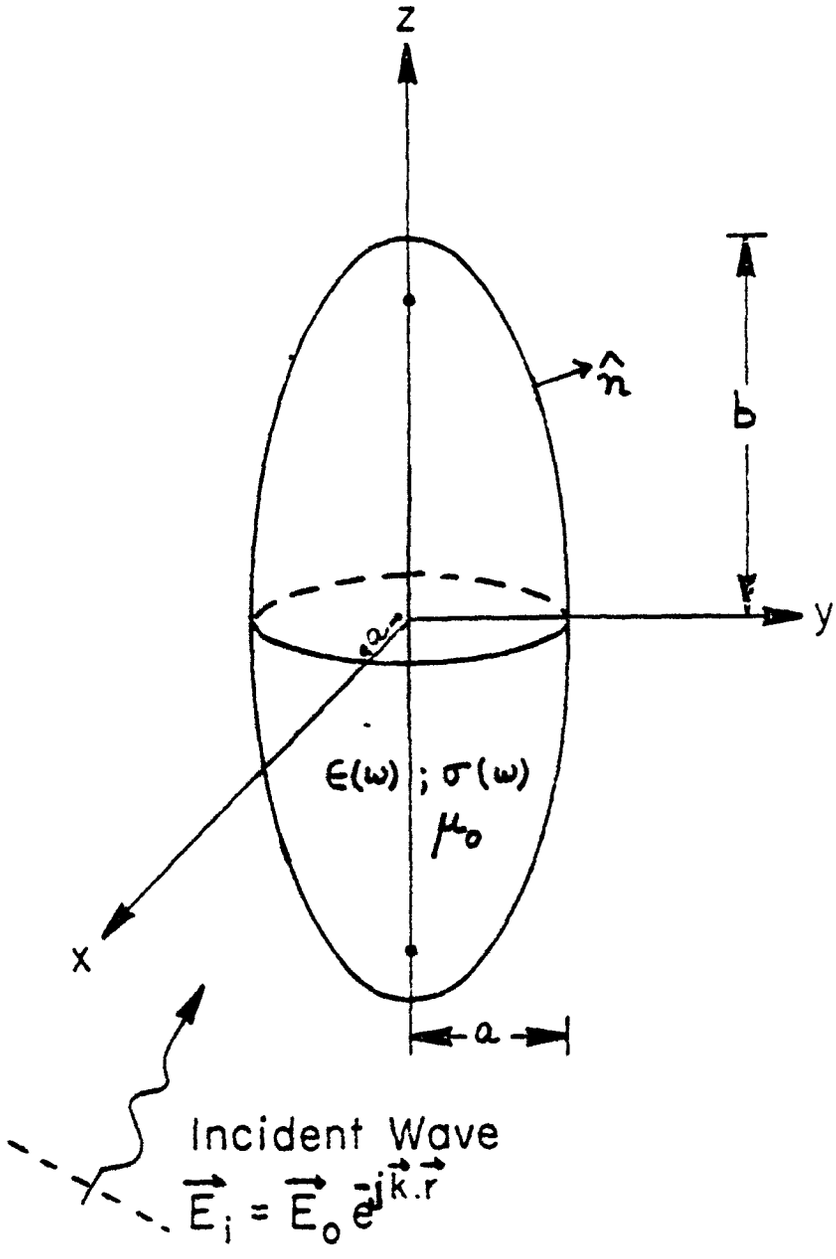

FIGURE 1. The Prolate Spheroidal Model

Knowing the internal field for a given incident radiation, the absorption pattern, total power absorbed and the absorption cross section can be easily calculated.

Numerous analytical techniques have been used to solve the problem of scattering by spheroidal and ellipsoidal objects including the classical separation of variables method, the series expansion approach of Stevenson, the point matching method using spherical wave functions and other methods derived from these. The degree of success of these methods, in terms of accuracy and economy, is dependent on the dielectric and conducting properties of the spheroid and its geometrical properties, e.g., eccentricity. We have applied the following techniques in an attempt to evaluate the absorption characteristics for realistic models of man and animals:

- Stevenson's Method in the Third Approximation
- Spheroidal Function Expansion Method
- Point Matching Technique
- Extended Boundary Condition Method (EBCM).

Of these, the Stevenson's method in the third approximation and EBCM were found to be most successful for the problem at hand. These methods are presented in detail in the following sections.

2-2. STEVENSON'S METHOD IN THE THIRD APPROXIMATION

As stated before, a low frequency analysis of power absorption by prolate spheroidal [8,9] and ellipsoidal [10,11] models has been conducted for nose-on and broadside-incidence only by utilizing Stevenson's method in the first approximation, and the results are known.

In this report it is shown that the electromagnetic power absorbed by the ellipsoidal model of man and animals, when radiated by a plane wave at an arbitrary angle of incidence, can be evaluated by applying Stevenson's analysis [12,13] in the third approximation. The frequency range of validity and the data accuracy can be improved by utilizing this third order solution for the model being considered. In addition, Stevenson's general formulation is applicable for any arbitrary angle of incidence.

According to this method, the problem was formulated by showing that the general solution of the electromagnetic problem can be expressed formally as a power series in the ratio of dimension to wavelength. Each term in the series then requires the solution of a standard problem in potential theory, the first solution being the quasi-static solution of Lord Rayleigh. Thus, if the geometry of the object is such that Laplace's equation can be solved in the appropriate coordinate system, the series can be continued arbitrarily although the terms become increasingly complicated. The method is completely general subject only to the range of validity over which the particular order of expansion applies. The method can be easily applied to the ellipsoidal models since the theory of ellipsoidal harmonics has been fairly extensively developed. Stevenson has applied this method in the third approximation to ellipsoids, and his results are used in this report to evaluate the power

absorption in uniform tissue models by utilizing the forward scattering theorem given by Van De Hulst [22]. The results obtained agree well with known results within the range of validity, which is approximately kc < 1, where c is the major axis.

2-2-1. Theoretical Formulation

Following Stevenson, the incident field is assumed to be:*

$$E^i = E_o(\ell_1, m_1, m_1)e^{ik(\ell x+my+nz)} \tag{6a}$$

$$H^i = E_o\sqrt{\frac{\varepsilon_o}{\mu_o}}\,(\ell_2, m_2, n_2)e^{ik(\ell x+my+nz)} \tag{6b}$$

where (ℓ,m,n), (ℓ_1,m_1,n_1) and (ℓ_2,m_2,n_2) are three sets of direction cosines satisfying the relation:

$$(\ell_1,m_1,n_1) = (\ell_2,m_2,n_2) \times (\ell,m,n)$$

$$(\ell_2,m_2,n_2) = (\ell,m,n) \times (\ell_1,m_1,n_1)$$

The expression for far-zone electric field components of the scattered field are [13]:

$$E_\theta^s = \left(\frac{\partial P}{\partial\theta} + \frac{1}{\sin\theta}\frac{\partial\overline{P}}{\partial\phi}\right)\frac{e^{ikR}}{R}\cdot E_o = \eta H_\phi \tag{7a}$$

$$E_\phi^s = \left(\frac{1}{\sin\theta}\frac{\partial P}{\partial\phi} - \frac{\partial\overline{P}}{\partial\theta}\right)\frac{e^{ikR}}{R}\cdot E_o = -\eta H_\theta \tag{7b}$$

Here (R,θ,ϕ) are the spherical polar coordinates of the field point and P and $\overline{P}$ are functions of the surface harmonics $S_j^{(m)}$ defined by:

$$P = \sum_{s=2}^{\infty} k^s \sum_{j=1}^{s-1} \frac{(-1)^j}{j(j+1)} S_j^{(s-j-1)} \tag{8a}$$

$$\overline{P} = \sum_{s=2}^{\infty} k^s \sum_{j=1}^{s-1} \frac{(-1)^j}{j(j+1)} \overline{S}_j^{(s-j-1)} \tag{8b}$$

For a three term series the expansion for P is reduced to:

---

* The time convention $e^{-i\omega t}$ rather than $e^{j\omega t}$ is used in this section to represent the harmonically oscillating fields.

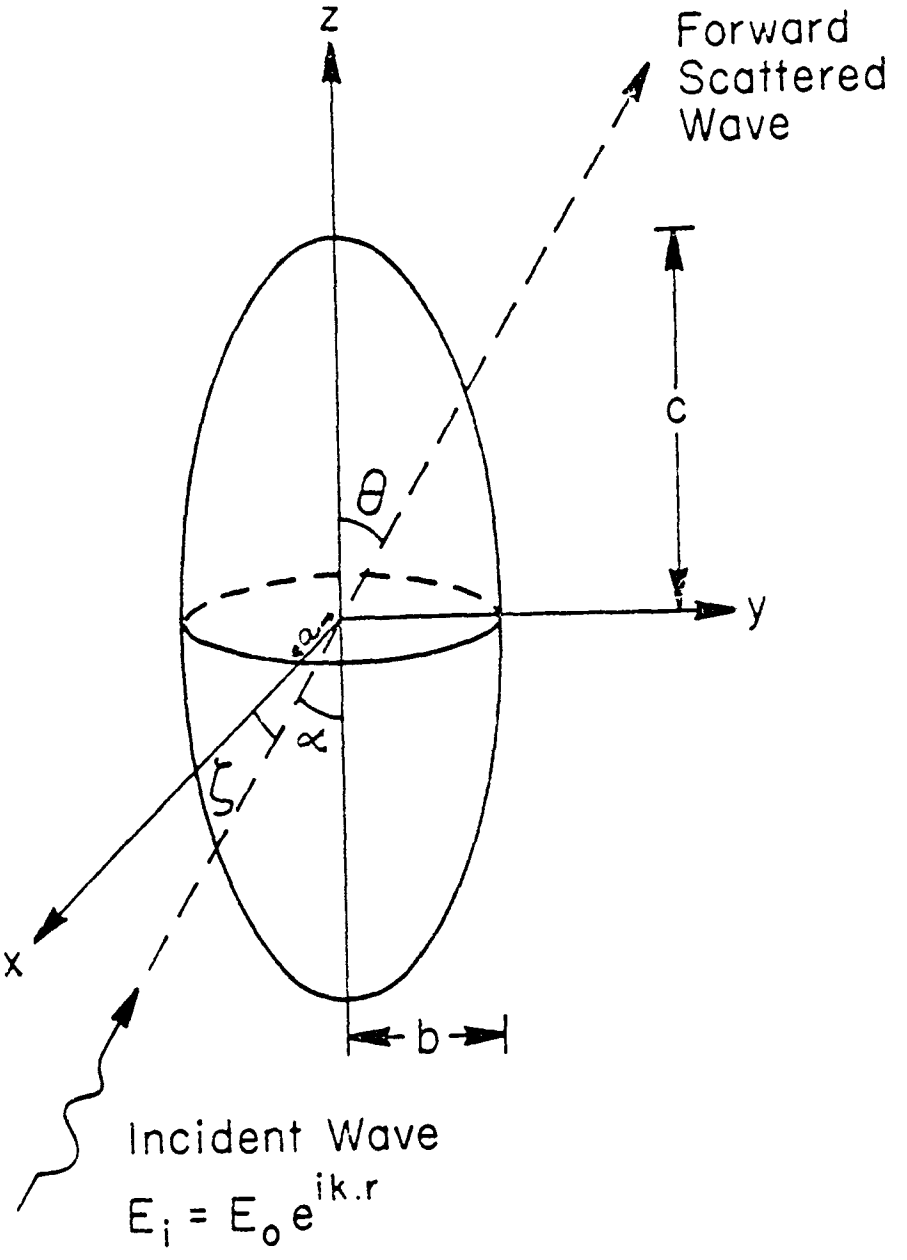

FIGURE 1'. The Uniform Tissue Ellipsoidal Model

$$P = k^2 \left[(K_1\cos\phi + K_2\sin\phi)\sin\theta + K_3\cos\theta\right] + k^4\{(L_1\cos\phi + L_2\sin\phi)\sin\theta$$

$$+ L_3\cos\theta + (M_1\cos^2\phi + M_2\sin^2\phi)\sin^2\theta + M_3\cos^2\theta + (N_1\sin\phi + N_2\cos\phi)\sin\theta\cos\theta$$

$$+ N_3\sin\phi\cos\phi\sin^2\theta - \frac{1}{30}\left[(K_1\cos\phi + K_2\sin\phi)\sin\theta + K_3\cos\theta\right]\left[\sin^2\theta(a^2\cos^2\phi\right.$$

$$\left. + b^2\sin^2\phi) + c^2\cos^2\theta\right]\} \quad (+ \text{ higher order terms}). \tag{9}$$

and $\overline{P}$ is obtained from P by making the substitution:

$$(\ell_1,m_1,n_1) \rightarrow (\ell_2,m_2,n_2)$$

$$(\ell_2,m_2,n_2) \rightarrow -(\ell_1,m_1,n_1) \text{ and } \varepsilon \leftrightarrow \mu. \tag{10}$$

That is, $\overline{P}$ is given by the same equation as (9) involving "barred" constants $\overline{K}$, etc. The scattering constants K_j, L_j, $\overline{K}_j$, $\overline{L}_j$, etc. with j = 1, 2 and 3 are functions of the semi-axes, ellipsoidal dielectric constant and permeability, direction cosines (ℓ,m,n), (ℓ_1,m_1,n_1) and (ℓ_2,m_2,n_2) and certain integrals. The defining expressions for these are given in Appendix A.

The power absorbed by the ellipsoidal model can be evaluated by utilizing the forward scattering theorem [22]. For a wave incident at an angle α making an angle ζ with respect to the x-z plane, as shown in Figure 1', the forward scattering amplitude is given as:

$$S(o) = \frac{1}{E_o}(\ell_1,m_1,n_1) \lim_{R\to\infty}\left[-ikRe^{-ikR}E^s\Big|_{\substack{\text{along the direction corresponding}\\ \text{to } \ell,m,n;\text{ i.e., along } \theta=\alpha \text{ and } \phi=\pi+\zeta}}\right] \tag{11}$$

Then the extinction cross section [22] is given by:

$$C_{ext} = \frac{4}{k^2}\ \mathrm{Re}[S(o)]\ . \tag{12}$$

The absorption cross section of the ellipsoid can then be determined in terms of the extinction cross section and the scattering cross section and is given by:

$$C_{abs} = C_{ext} - C_{sca} \tag{13}$$

Where C_{sca}, the scattering cross section is defined as the ratio of power scattered by the ellipsoid to the power incident per unit area and is given by:

$$C_{sca} = \frac{2\eta}{E_o^{\ 2}} \cdot \int_{\theta=0}^{\pi}\int_{\phi=0}^{2\pi} \frac{1}{2}\,\mathrm{Re}[E \times H^*] \cdot R^2\sin\theta d\theta d\phi. \tag{14}$$

Substitution of equation (7) leads to [2]:

$$C_{sca} = \frac{8\pi}{3} k^4 \sum_{j=1}^{3} (|K_j|^2 + |\overline{K}_j|^2) + \frac{16\pi}{3} k^6 \{\mathrm{Re} \sum_{j=1}^{3} (K_j L_j^* + \overline{K}_j \overline{L}_j^*)$$

$$- \frac{1}{150} [(3a^2 + b^2 + c^2)(|K_1|^2 + |\overline{K}_1|^2) + (3b^2 + c^2 + a^2)(|K_2|^2 + |\overline{K}_2|^2)$$

$$+ (3c^2 + a^2 + b^2)(|K_3|^2 + |\overline{K}_3|^2)]\} + \text{higher order terms.} \qquad (15)$$

The power absorbed by uniform lossy spheroidal and ellipsoidal models can then be easily calculated by evaluating the coefficients given in Appendix A for specified ε and μ and using equations (12), (13) and (15). For uniform tissue models considered here $\mu=1$ and $\varepsilon=\varepsilon'+i\varepsilon''=\varepsilon'-i\ (\sigma/\omega\varepsilon_0)$. Dielectric values for high water content tissues are given by Johnson and Guy [4].

2-2-2. Comparison With Long Wavelength Results [8-11]

Examination of the expressions obtained for the absorption cross section reveals that for nose-on (n=1, incident radiation along z-axis) and broadside (ℓ=1 or m=1; i.e., incident radiation along x- or y-axis) incidence, the derived expressions can be reduced to those obtained for spheroidal and ellipsoidal models [8-11] if the higher order terms are neglected and if it is assumed that for the tissue model, $-\varepsilon''=(\sigma/\omega\varepsilon_0) >> \varepsilon' >> 1$. For example, for the ellipsoidal model with E K H incidence $\ell_1=m=n_2=1$, substituting into the expressions for scattering coefficients (Appendix A) and retaining only the dominant terms in the expressions for C_{abs} leads to:

$$C_{abs} \cong -\frac{4\pi}{k} \mathrm{Im}[k^2 K_1 - k^4 \overline{L}_3] \qquad (16)$$

where

$$K_1 = \frac{2}{3} (\varepsilon-1) f_1(\varepsilon), \qquad (17a)$$

and

$$15\overline{L}_3 = -f_3(\mu)b^2 - f_3^2(\mu)\varepsilon \frac{a^2 + b^2}{abc} + f_3^2(\mu)g_3(\varepsilon) \{(I_a - I_b) [-\frac{\varepsilon}{2}(a^2 + b^2)$$

$$+ b^2 + \varepsilon \frac{a^2 - b^2}{abc}\} - f_3^2(\mu)g_3(\varepsilon) \{(I_a - I_b)\varepsilon(\varepsilon - 2) \frac{a^2 - b^2}{abc}\} \qquad (17b)$$

with

$$f_1(\varepsilon) = [(\varepsilon - 1)I_a + \frac{2}{abc}]^{-1}; \quad f_3(\mu) = \frac{abc}{2};$$

$$g_3(\varepsilon) = [(\varepsilon - 1)(a^2 + b^2)I_{ab} + \frac{2}{abc}]^{-1} \text{ and } I_{ab} = (I_a - I_b)/(b^2 - a^2).$$

Utilizing the property of the tissue model that $\varepsilon >> 1$ and retaining only the dominant terms in K_1 and $\bar{L}_1$ gives:

$$\text{Im } K_1 \cong \frac{4}{3 \text{ abc } I_a^2 \varepsilon''} \tag{18a}$$

$$\text{Im } \bar{L}_3 \cong \frac{1}{15} [- \frac{abc}{4} \varepsilon''(a^2 + b^2) + \frac{abc}{4} \varepsilon'' \frac{(a^2 - b^2)^2}{(a^2 + b^2)}]$$

$$= - \frac{abc}{15} \varepsilon'' \frac{a^2 b^2}{(a^2 + b^2)} \quad . \tag{18b}$$

Substituting $-\varepsilon'' = \sigma/\omega\varepsilon_o$ and equations (13a-b) into (11) and using:

$$P_{av} = (\frac{1}{2\eta} E_o^2 C_{abs}/\text{volume of the ellipsoid}) \text{ leads to:}$$

$$P_{av} = \frac{1}{2} \sigma E_o^2 k^2 [A_x^2 - a^2 \frac{B_z}{5}] \tag{19}$$

where $$A_x^2 = [\sigma^2 \eta_o^2 (\frac{abc}{2})^2 I_a^2]^{-1} \text{ and } B_z = - \frac{b^2}{a^2 + b^2}$$

which is identical to the result obtained by Massoudi et al [10] for E K H incidence. Similarily, for other cases of both nose-on and broadside incidence it is seen that the expression for absorbed power reduces to the ones for prolate spheroidal [8] and ellipsoidal models [10] if the higher order terms are neglected and it is assumed that $\sigma/\omega\varepsilon_o >> \varepsilon' >> 1$. This amounts to retaining only the dominant terms in the extinction cross section and neglecting the scattered energy which is implicitly assumed in the long-wavelength analysis.

2-2-3. Prolate Spheroidal Model

For the prolate spheroidal uniform tissue model $a = b < c$. Then,

$$I = \frac{1}{(c^2 - a^2)^{1/2}} \ln \frac{c + (c^2 - a^2)^{1/2}}{c - (c^2 - a^2)^{1/2}} \tag{20}$$

and the remaining integrals can be calculated in terms of I by using the relations connecting the elliptic integrals as given in Appendix A. The scattering constants for the three cases of polarization (a) nose-on with n=1 and b) broadside with m=1 and either ℓ_1=1 or n_1=1) are given in Appendix B. The

tissue is characterized by $\mu=1$ and $\varepsilon=(\varepsilon'-i\sigma/\omega\varepsilon_o)$. The values of ε' and σ used in the calculations are the same as those given by Johnson and Guy [4]. It can be easily shown that scattering constants in Appendix B lead to the same expression for power absorbed by the model as that derived by Durney et al [8] if the higher order terms in P and $\overline{P}$ are neglected for the case of $\sigma/\omega\varepsilon_o >> \varepsilon' >> 1$. That is, the expressions derived in [8] approximately correspond to:

$$C_{abs} \simeq C_{ext} \simeq -\frac{4\pi}{k} \mathrm{Im}[K_1 - \overline{L}_3] \tag{21a}$$

for $m = \ell_1 = -n_2 = 1$ (or magnetic polarization case)

$$C_{abs} \simeq C_{ext} \simeq -\frac{4\pi}{k} \mathrm{Im}[K_1 + \overline{L}_2] \tag{21b}$$

for $n = \ell_1 = m_2 = 1$ (or cross polarization case)

$$C_{abs} \simeq C_{ext} \simeq -\frac{4}{k} \mathrm{Im}[K_3 + \overline{L}_1] \tag{21c}$$

for $m = n_1 = \ell_1 = 1$ (or electric polarization case).

2-3. POINT MATCHING METHOD

The problem of the scattering and absorption characteristics of rain drops has been formulated by Oguchi [15] and Morrison and Cross [16]. The technique can be extended with certain limitations to the case of prolate spheroidal models of man and animals. For the point matching technique, the incident, scattered and internal fields are expanded in terms of the spherical vector wave functions with known coefficients of expansion for the incident wave. The boundary conditions are then applied at a number of points (larger than the number of unknown coefficients of expansion to be evaluated) on the surface of the prolate spheroid ($r=ab/(a^2\cos^2\theta+b^2\sin^2\theta)^{1/2}$, with a the major and b the minor axis) and the coefficients are then computed by using the least square fitting procedure [23]. This leads to better accuracy as compared to the case where the boundary conditions are applied to a number of points equal to the number of unknown coefficients. A computer subroutine to compute a least square fit for a linear system with complex coefficients was written and attempts were made to solve for the coefficients of expansion using this technique. The accuracy of the results obtained can, of course, be checked by using the solutions obtained to compute the boundary conditions fit at points other than those used to obtain the coefficients of expansion.

2-4. SEPARATION OF VARIABLES METHOD

This method follows the analytical technique developed by Asano and Yamamoto [17] who have formulated the problem of light scattering by small particles in terms of vector spheroidal wave functions. The fields in the three regions are expanded in terms of the spheroidal vector wave functions [24]. The boundary conditions are then applied at the surface by defining auxilliary

spheroidal angle functions [17] which enables one to apply the boundary conditions to the tangential components of the electric and magnetic fields at $\zeta=\zeta_o$ resulting in a system of coupled equations for the expansion coefficients. The coefficients are then calculated by truncating the series. A computer subroutine to calculate the spheroidal angle functions with complex arguments has been written which together with known results for spheroidal functions with real arguments leads to the evaluation of the coefficients of expansion.

2-5. EXTENDED BOUNDARY CONDITION METHOD

The extended boundary condition method (EBCM) was formulated by Barber and Yeh [18] to evaluate the scattering by arbitrarily shaped dielectric objects by utilizing Schelkunoff's equivalence theorem. The method has been applied by Barber [19] to evaluate the absorption characteristics of prolate spheroidal models in the resonance region. According to this method, as far as the external fields are concerned, the object can be replaced by a set of surface currents. These surface currents are such that the fields inside are zero, i.e., the field produced by these currents exactly cancels the internal fields resulting in an equation relating the internal fields to the surface currents (or the tangential components of the fields just outside the surface). Applying the boundary conditions at the surface leads to a linear system of integral equations for the coefficients of the unknown internal field in terms of the known coefficients of the incident field. Knowing the internal fields, the scattered field can be determined in terms of the surface fields (or currents). The absorption cross section can then be determined by utilizing the forward scattering theorem of Van De Hulst [22] or by integrating the incremental internal power distribution σE_i^2 in the object.

The analytical technique is outlined in Appendix C for convenience. It is basically the same as that used by Barber [19] except for some minor modifications, such as the utilization of complex linear combinations of even- and odd-vector wave functions for computational convenience and efficiency.

The program flow chart and program listing is also appended, Appendix D.

SECTION 3

NUMERICAL RESULTS

The absorption cross section of various models of man and animals was evaluated as a function of frequency and the angle of incidence by utilizing various techniques outlined in the previous section. Each technique was found to be implementable only over a limited range of frequencies and object properties and dimensions. For example, numerical results using point matching and spheroidal wave function methods converged only for a class of unrealistic models having low eccentricities, i.e., $b/a < 2$ and/or having conductivities much less than the high water content tissue medium. The cylindrical functions with complex argument (dependent on the object dimensions and complex dielectric constant) undergo an enormous variation in magnitude as one moves on the surface from a point on the minor axis to one on the major axis, resulting in a rather ill-conditioned set of linear equations and nonconverging numerical solutions. We should add that the point matching method has been successfully formulated and applied by us to evaluate the absorption characteristics of objects with relatively low eccentricities where the variation in the coefficients of the system of linear equations for unknown coefficients of expansion is relatively small. The results obtained using the point matching techniques were the same as those subsequently published by Ruppin [27] for near spherical objects.

The absorption cross sections for some typical cases of man and animal prolate spheroidal models was calculated by utilizing Stevenson's method in the third approximation as given in Section 2-2 and the extended boundary method for which the computer program is described in Appendix D. The results obtained for a rhesus monkey model in the third approximation are shown in Figure 2 for the three standard cases of incident wave polarization. The absorption cross section calculated by utilizing the extended boundary condition method (EBCM) is shown in Figure 3 and as seen, the results obtained by utilizing Stevenson's formulation in the third approximation are in excellent agreement with the ones obtained by EBCM within the range of validity of the third order solution. The EBCM results agree well with those of Barber [19] except that they do indicate a well defined resonance for E incidence at a slightly lower frequency for the rhesus monkey model.

Figure 4 shows the variation in the absorption cross section near the resonance frequency of the rhesus monkey model as a function of the angle of incidence of the plane wave for the two possible polarization cases (magnetic or electric field parallel to the minor axis). These results were computed by EBCM and as expected, they indicate that the absorption cross section increases

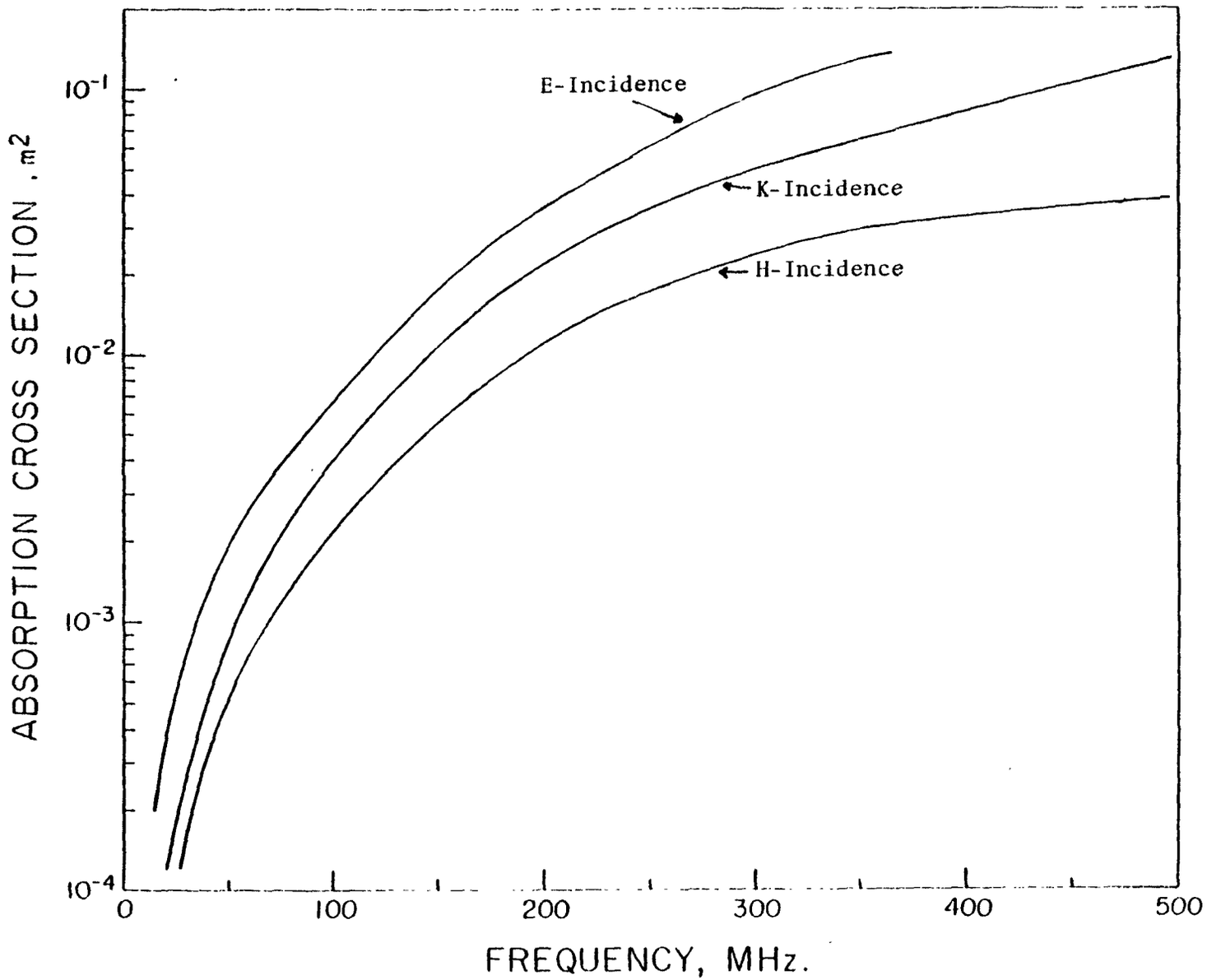

FIG.2. Absorption Cross Section of a Prolate Spheroidal Model of Rhesus Monkey Results in the third approximation;c,major semi axis=0.2m,c/b=3.09.

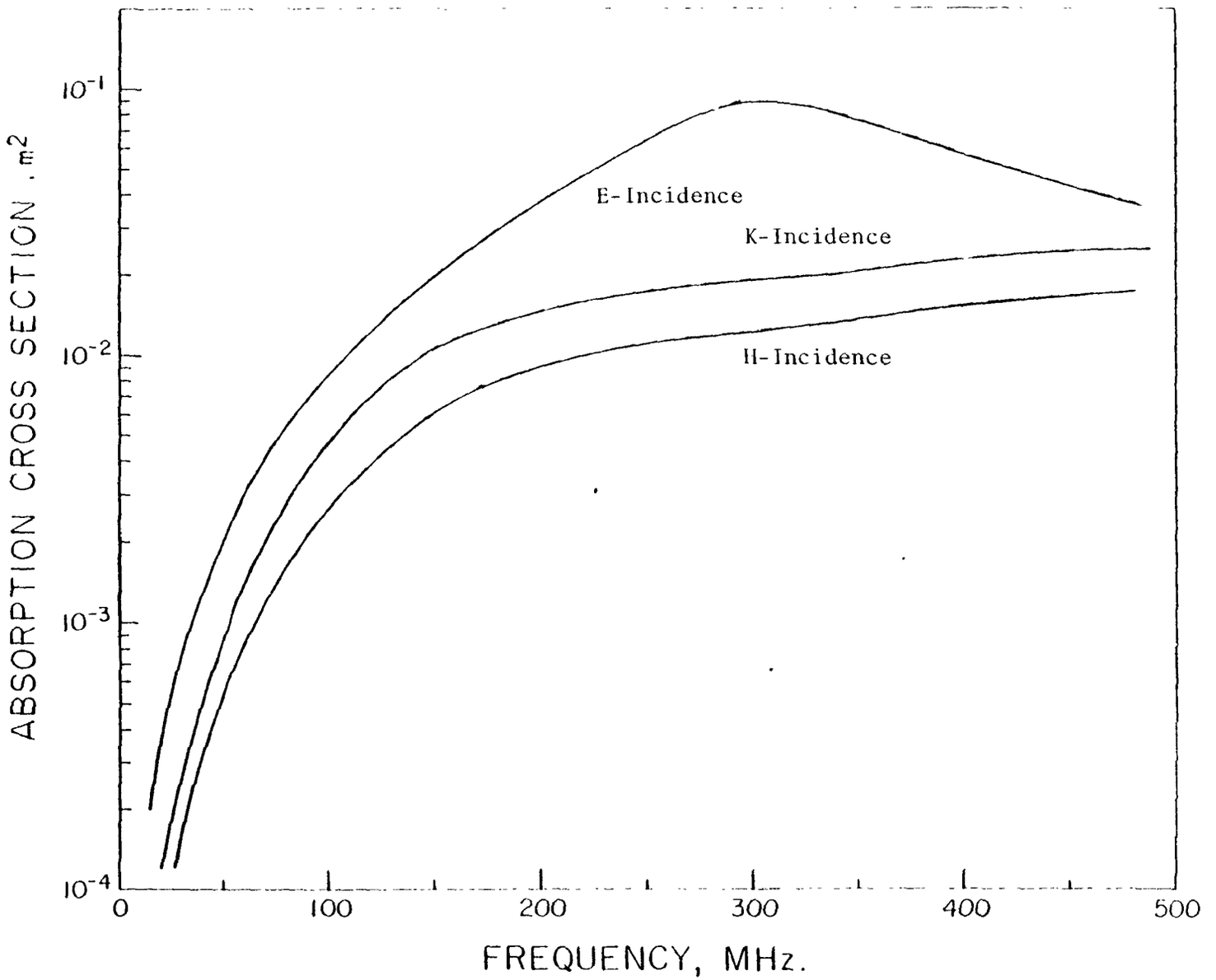

FIG.3. Absorption Cross Section of a Prolate Spheroidal Model of Rhesus Monkey Results using EBCM; c,major semi axis=0.2m, c/b=3.09.

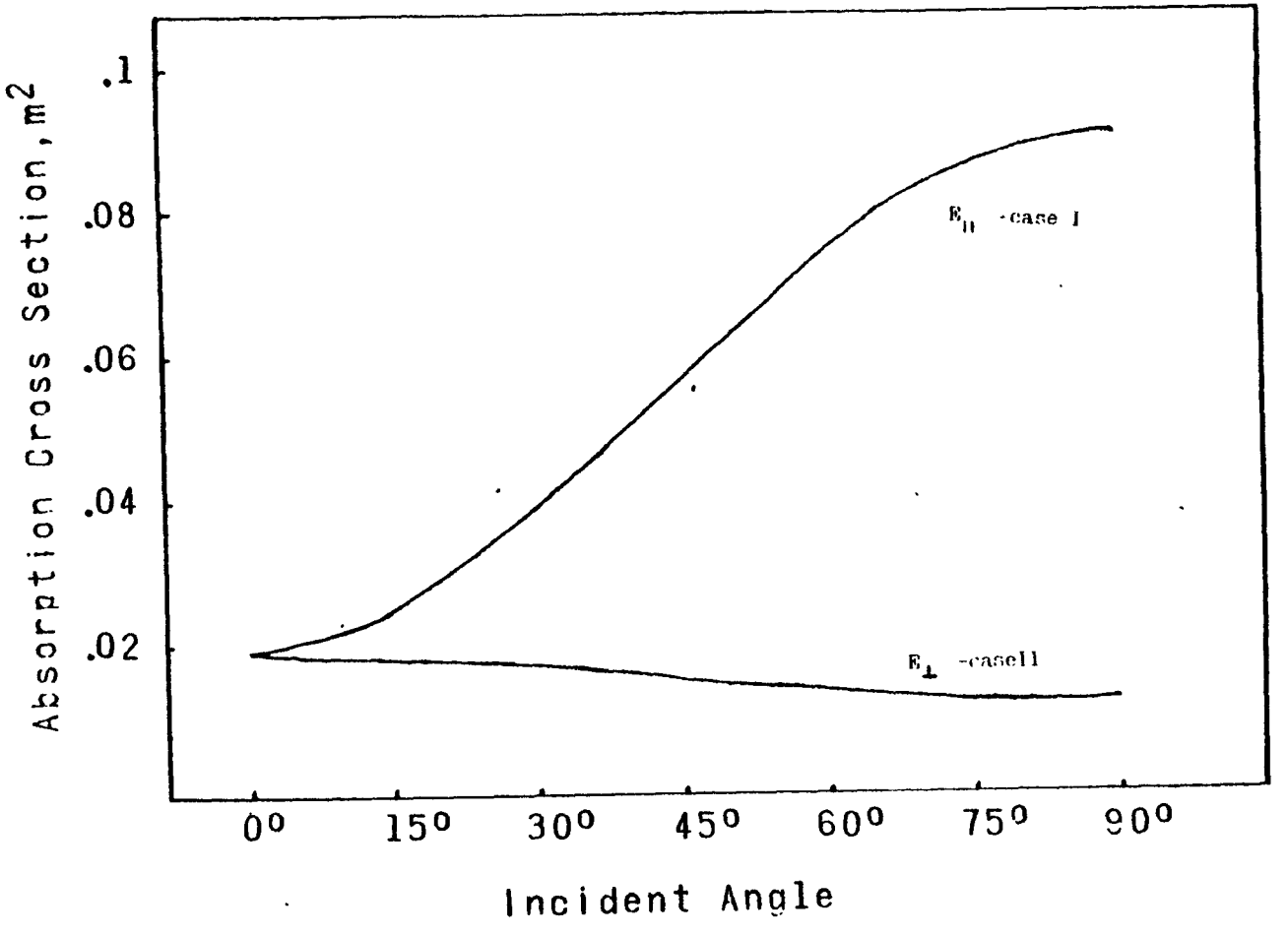

Figure 4. Absorption Cross Section of the Rhesus Monkey Model as a Function of the Incident Angle of Radiation at Resonance- Results using EBCM.

as the component of electric field along the major axis increases. The results obtained for other prolate spheroid models and the ones obtained by using Stevenson's method exhibit similar behavior.

The absorption cross section for average man model is shown in Figure 5. For these models representing average man as a prolate spheroidal object consisting of high water content tissue material, the EBCM numerical technique did not result in converging solutions beyond about 80 MHz for the two polarization cases in which the E field is parallel to the minor axis and not beyond about 30 MHz for the case in which the E field lies along the major axis of the spheroid, as shown in Figure 5. This is due to the fact that the matrices became ill-conditioned for larger values of conductivity and/or spheroid eccentricity. However, the absorption characteristics can be estimated by means of an extrapolation method, as used by Barber [19] who seemed to have had similar difficulty regarding convergence of solutions for uniform tissue prolate spheroidal models of man. The solutions in the third approximation for the average man model for the case of incident wave polarized along the major axis do not converge beyond 50 MHz. However, the solution does converge for lower values of dielectric constants. For example, the absorption cross section for normalized dielectric constant = (0.1) x (ε_{tissue}) is shown in Figure 6. It is in excellent agreement with the results obtained by Barber [19] who has calculated the absorption cross section for spheroidal model with normalized dielectric constants and used them to extrapolate and estimate absorption beyond 30 MHz for E parallel to major axis incidence. The dashed curve for the E parallel incidence case in Figure 5 is an estimated solution in the third approximation obtained by the same extrapolation procedure. Examination of these results indicates that, in general, the solution in the third approximation is valid up to approximately kc = 1 for most cases. It should be noted that there is no significant improvement in accuracy at low frequencies for high water content uniform tissue prolate spheroidal models in the third approximation as compared to the results obtained by using the long wave length, first order analysis for the three cases of wave polarization. This should reinforce the accuracy of the results presented for ellipsoidal models by Massoudi et al [10,11]. However, at higher frequencies or with objects where the condition $\sigma/\omega\varepsilon >> \varepsilon' >> 1$ is no longer valid (e.g., Figure 6); the analysis in the third approximation leads to more accurate results.

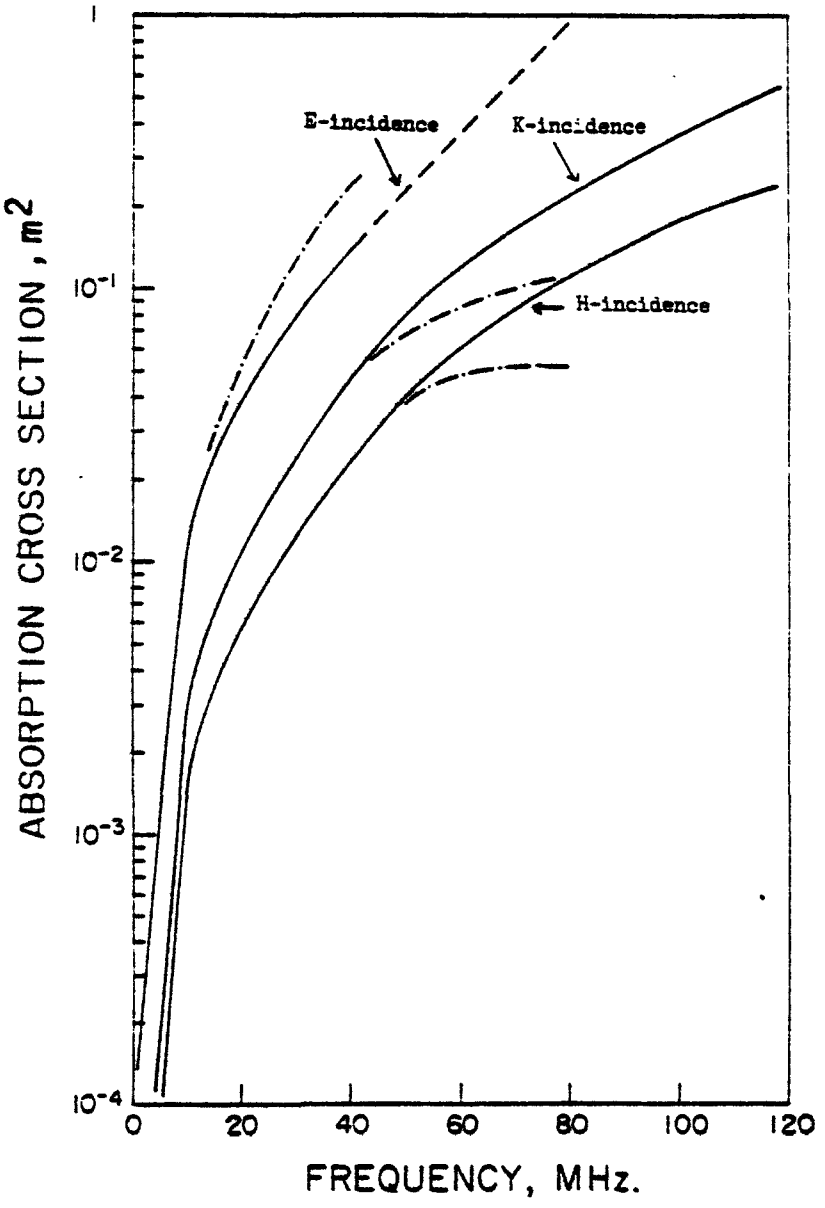

Figure 5. Absorption cross section of a prolate spheroidal model of an average man. c=0.875 m, c/b = 6.34.
—— results in the third approximation.
-·-·-·results using EBCM
---- estimated values in the third approximation

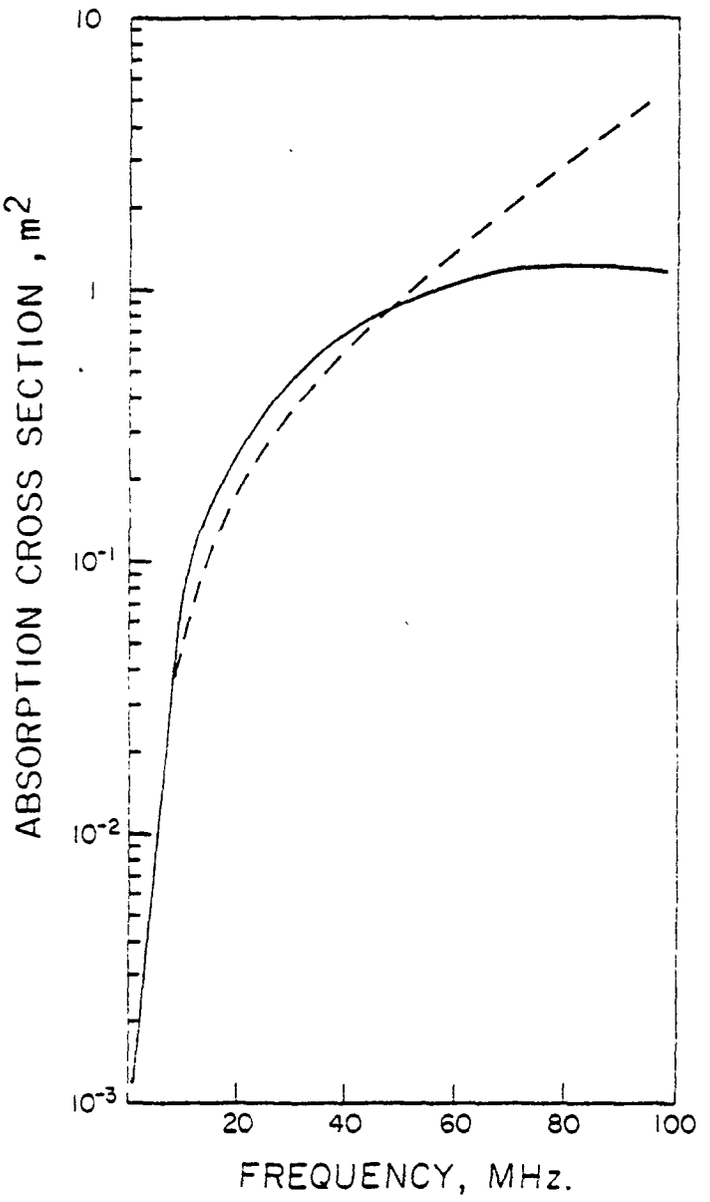

Fig.6. Absorption Cross Section of a Prolate Sheroidal Model with $\epsilon = 0.1\,\epsilon_{tissue}$, c=0.875m, c/b=6.34; E-parallel incidence.
——— results in the third approximation
- - - - - results using the long wavelength theory.

SECTION 4

CONCLUSIONS AND SUGGESTIONS FOR FURTHER STUDY

4-1. CONCLUSIONS

In an attempt to evaluate the absorption characteristics of prolate spheroidal models of man and animals at and near the resonance frequencies, several techniques, including Stevenson's method in the third approximation and the extended boundary condition method, have been utilized. Even though the absorption cross sections for many animal models with low eccentricities could be evaluated at and beyond the resonance frequency, application of these methods to high eccentricity models lead to nonconverging solutions and ill-conditioned matrices above certain frequencies. This includes the important case of the prolate spheroidal model of average man consisting of high water content tissues. The results obtained agree well with known results within the range of validity of the two methods.

Stevenson's method in the third approximation developed in this report in Section 2-2 provides a simple direct approach to the evaluation of absorption characteristics of both prolate spheroid and ellipsoid models radiated by plane waves at an arbitrary angle of incidence up to approximately $kc = 1$, where c is the major axis. Earlier work to date on the low frequency analysis [8-11] has been applicable in the first approximation to the problem of the absorption by prolate spheroidal and ellipsoidal models and other objects with $\sigma >> \omega\varepsilon$ and for nose-on and broadside-incidence only. The technique presented in the report is more general and accurate and can be applied to objects having arbitrary electrical properties, e.g., raindrops and other particles subjected to radiation at arbitrary angle of incidence. The accuracy and frequency range of validity for low frequency solutions has been extended through this work by considering higher order terms.

The extended boundary condition method of Barber was also utilized to evaluate the absorption characteristics of prolate spheroidal models. After a careful investigation of other techniques, it was concluded that this method was the most amenable one for obtaining solutions at higher frequencies. Even though the analytical procedure is basically the same as formulated by Barber, we have formulated the computational technique with modifications, such as the utilization of even- and odd-vector wave functions and have utilized improved subroutines in an attempt to find more accurate solutions with improved computational efficiency. For example, our results showed that for some animal models, resonance occurs at a slightly lower frequency than that obtained by Barber (e.g., Figure 3 for rhesus monkey). In addition, this work represents

an independent source of confirmation, and the results can be used to evaluate the absorption cross sections of any prolate spheroidal model not available in the literature.

Only typical solutions obtained for various models have been presented in the report. No attempt was made to compile the results for various models of man and animals since the results obtained exhibit similar behavior as those given in the report and can be easily evaluated by utilizing the third order approximation analysis given in Section 2-2, and the EBCM computer program described in Appendix D.

4-2. SUGGESTIONS FOR FURTHER WORK

A. A direct extension of the work would be the inclusion of even higher order terms in the analysis using Stevenson's method. This approach, though time-consuming and complicated, will extend the frequency range over which the solutions are valid.

B. Attempts should be made to formulate a computational technique by which the so-called ill-conditioned matrix obtained at resonant frequency using the EBCM method for high eccentricity models can be avoided. One such approach might be to improve precision by solving the equations after separating them into real and imaginary parts. The single word accuracy of the Cyber machine used in our computations is 15 digits, and the double precision for complex variables is not provided. It is believed that by providing such a double precision for complex variables, the frequency range over which the solutions can be found can be increased for a given model.

C. Attempts should be made to formulate analytical techniques which lead to converging solutions near resonance for high eccentricity high water content tissue models. One possible approach would be to formulate Schellkuneff's equivalence principle, which is the foundation of the EBCM method in terms of spheroidal vector wave functions. Such an approach might lead to converging solutions.

D. Attempts should be made to incorporate various realistic boundary conditions in analyses involving prolate spheroid or ellipsoidal models. One useful problem would be to evaluate the effect of the earth's surface on the absorption characteristics of various models. Another important problem is the evaluation of the absorption characteristics of the models placed in guided wave structures, such as the rectangular coaxial structures. Such structures have been used to measure the absorption characteristics of various models as well as experimental animals.

REFERENCES

1. Anne, A., et al., "Relative Microwave Absorption Cross Section of Biological Significance," in Biological Effects of Microwave Radiation, Vol. 1, pp 153-176, New York, Plenum; 1960.

2. Shapiro, A. R., et al., "Induced Fields and Heating Within a Cranial Structure Irradiated by an Electromagnetic Plane Wave," IEEE Trans. Microwave Theory Tech., Vol. MTT-19, pp 187-196; February 1971.

3. Kritikos, H. N. and Schwan, H. P., "Hot Spots Generated in Conducting Spheres by Electromagnetic Waves and Biological Implications," IEEE Trans. Bio-Med. Eng., Vol. BME-19, pp 53-58; January 1972.

4. Johnson, C. C. and Guy, A. W., "Nonionizing Electromagnetic Wave Effects in Biological Materials and Systems," Proc. IEEE, Vol. 60, pp 692-718; June 1972.

5. Joines, W. T. and Spiegel, R. J., "Resonance Absorption of Microwaves with Human Skull," IEEE Trans. Bio-Med. Eng., Vol. BME-21, pp 46-48; January 1974.

6. Weil, C. M., "Absorption Characteristics of Multi-Layered Sphere Models Exposed to UHF/Microwave Radiation," IEEE Trans. Bio-Med. Eng., Vol. BME-22, pp 468-476; November 1975.

7. Lin, J. C., et al., "Power Deposition in a Spherical Model of Man Exposed to 1-20 MHz Electro-magnetic Fields," IEEE Trans. Microwave Theory Tech., Vol. MTT-21, pp 791-797; December 1973.

8. Durney, C. H., et al., "Long-Wavelength Analysis of Plane Wave Irradiation of a Prolate Spheroid Model of Man," IEEE Trans. Microwave Theory Tech., Vol. MTT-23, pp 246-253; February 1975.

9. Johnson, C. C., et al., "Long-Wavelength Electromagnetic Power Absorption in Prolate Spheroidal Models of Man and Animals," IEEE Trans. Microwave Theory Tech., Vol. MTT-23, pp 739-747; September 1975.

10. Massoudi, H., et al., "Long-Wavelength Analysis of Plane Wave Irradiation of an Ellipsoidal Model of Man," IEEE Trans. Microwave Theory Techn., Vol. MTT-25, pp 41-46; January 1977.

11. Massoudi, H., et al., "Long-Wavelength Electromagnetic Power Absorption in Ellipsoidal Models of Man and Animals," IEEE Trans. Microwave Theory Tech., Vol. MTT-25, pp 47-52; January 1977.

12. Stevenson, A. F., "Solution of Electromagnetic Scattering Problems as Power Series in the Ratio: Dimension of Scatterer/Wavelength," Jour. Appl. Phys., Vol. 24, pp 1134-1142; September 1953.

13. Stevenson, A. F., "Electromagnetic Scattering by an Ellipsoid in the Third Approximation," Jour. Appl. Phys., Vol. 24, pp 1143-1151; September 1953.

14. Van Bladel, J., "Electromagnetic Fields," McGraw-Hill; 1964.

15. Oguchi, T., "Scattering Properties of Oblate Raindrops and Cross Polarization of Radio Waves Due to Rain: Calculations at 19.3 and 34.8 GHz," Jour. Radio Res. Labs., Vol. 20, pp 79-118; 1973.

16. Morrison, J. A. and M. J. Cross, "Scattering of a Plane Electromagnetic Wave by Axisymmetric Raindrop," Bell Syst. Techn. J., pp 955-1019; July-August 1974.

17. Asano, S. and G. Yamamoto, "Light Scattering by a Spheroidal Particle," Appl. Optics, pp 29-49; January 1975.

18. Baber, P. and C. Yeh, "Scattering of Electromagnetic Waves by Arbitrary Shaped Dielectric Bodies," Applied Optics, Vol. 14, pp 2864-2872, December 1975.

19. Barber, P. W., "Resonance Electromagnetic Absorption by Nonspherical Dielectric Objects," IEEE Trans. Microwave Theory Tech., Vol. MTT-25, pp 373-381; May 1977.

20. Schwan, H. P. and K. Li, "Hazards Due to Total Body Radiation," Proc. IRE, Vol. 44, pp 1572-1581; November 1956.

21. Livesay, D. E. and K. M. Chen, "Electromagnetic Fields, Induced Inside of Biological Bodies," IEEE-S-MTT, Intl. Microwave Symp. Digest, pp 35-37; 1974.

22. Van De Hulst, H. C., "Light Scattering by Small Particles," Wiley; 1957.

23. Businger, P. and G. H. Golub, "Linear Least Squares Solutions by Householder Transformations," Numer. Math., 7, pp 269-276; September 1965.

24. Flammer, C., "Spheroidal Wave Functions," Stanford Univ. Press; 1957.

25. Strattan, J. A., "Electromagnetic Theory," McGraw-Hill; 1974.

26. Morse, P. M. and H. Feshbach, "Methods of Theoretical Physics," McGraw-Hill; 1963.

27. Rupin, R., "Calculation of Electromagnetic Energy Absorption in Prolate Spheroids by Point Matching Method," IEEE Trans. Microwave Theory and Tech., Vol. MTT-26, pp 87-90; February 1978.

APPENDIX A

SCATTERING COEFFICIENTS

The expressions for the scattering coefficients in equation (4) are given by:

$$K_1 = \frac{2}{3}(\varepsilon - 1)f_1(\varepsilon)\ell_1 \tag{A1}$$

$$\begin{aligned}
15L_1 = {} & f_1(\varepsilon)\{(\varepsilon - 1)\ell_1[\tfrac{1}{3}(6a^2 - b^2 - c^2) - (a^2\ell^2 + b^2m^2 + c^2n^2)] \\
& + \varepsilon(b^2mn_2 - c^2nm_2)\} + f_1{}^2(\varepsilon)\ell_1\{(\varepsilon - 1)[(\varepsilon - 2)I \\
& + \varepsilon a^2 I_a - \frac{4a}{bc}] + \varepsilon^2\mu(b^2 + c^2)/(a\ b\ c)\} + f_1(\varepsilon)g_1(\mu) \\
& x\{(I_b - I_c)[\tfrac{\mu}{2}(b^2 + c^2)(mn_2 + nm_2) - mn_2b^2 - nm_2c^2] \\
& -\varepsilon\mu(b^2 - c^2)(mn_2 + nm_2)/(a\ b\ c)\} + f_1{}^2(\varepsilon)g_1(\mu)\ell_1 \\
& x\{(I_b - I_c)[(\varepsilon - 1)K_1(\mu) + \varepsilon\mu(\varepsilon\mu - 2)(b^2 - c^2)/(a\ b\ c)]\}
\end{aligned} \tag{A2}$$

$$\begin{aligned}
15M_1 = {} & \frac{\varepsilon - 1}{3Q}[(\varepsilon - 1)(I_{ab}nn_1 + I_{ac}mm_1 - 2I_{bc}\ell\ell_1) + \frac{2\varepsilon}{abc(\Sigma a^2b^2)} \\
& x(2a^2\ell\ell_1 - b^2mm_1 - c^2nn_1)]
\end{aligned} \tag{A3}$$

$$\begin{aligned}
15N_1 = {} & -\frac{1}{3}(\mu - 1)f_1(\mu)(b^2 - c^2)\ell_2 + g_1(\varepsilon)[(\varepsilon/2)(b^2 + c^2) \\
& x(mn_1 + nm_1) - b^2mn_1 - c^2nm_1] + f_1(\mu)g_1(\varepsilon) \\
& x\ell_2[\varepsilon\mu(b^2 - c^2)/(a\ b\ c) - (\mu - 1)k_1(\varepsilon)] \ .
\end{aligned} \tag{A4}$$

In the above expressions, the undefined functions and integrals are:

$$I_a = \int_0^\infty \frac{du}{(a^2 + u)R(u)}$$

$$R(u) = [(a^2 + u)(b^2 + u)(c^2 + u)]^{1/2}$$

$$I_{ab} = \int_0^\infty \frac{du}{(a^2 + u)(b^2 + u)R(u)}$$

$$f_1(\varepsilon) = [(\varepsilon - 1)I_a + \frac{2}{abc}]^{-1}$$

$$g_1(\mu) = [(\mu - 1)(b^2 + c^2)I_{bc} + \frac{2}{abc}]^{-1}$$

$$k_1(\varepsilon) = b^2 I_b - c^2 I_c - \frac{\varepsilon}{2}(b^2 + c^2)(I_b - I_c)$$

$$Q = (\varepsilon - 1)^2(I_{ab}I_{bc} + I_{bc}I_{ca} + I_{ca}I_{ab}) \frac{-4\varepsilon(\varepsilon - 1)}{abc}(J + \frac{\Sigma^2 a}{\Sigma a^2 b^2} J')$$

$$+ \frac{4\varepsilon^2}{a^2b^2c^2(\Sigma a^2 b^2)}$$

$$J = \int_0^\infty \frac{du}{[R(u)]^3} = (I_{ab} - I_{ac})/(c^2 - b^2)$$

$$J' = \int_0^\infty \frac{u\,du}{[R(u)]^3} = I_{ab} - c^2 J \quad \text{etc.}$$

$$\Sigma a^2 = a^2 + b^2 + c^2 \qquad \Sigma a^2 b^2 = a^2b^2 + b^2c^2 + c^2a^2.$$

The remaining scattering coefficients K_2, K_3, L_2, L_3, M_2, M_3 and N_2, N_3 in equation (4) are obtained by cyclic permutations of a, b, c; ℓ, m, n; ℓ_1, m_1, n_1; and ℓ_2, m_2, n_2.

The scattering coefficients referring to magnetic field $\overline{K}_j$, $\overline{L}_j$, $\overline{M}_j$ and $\overline{N}_j$ (j = 1, 2, 3) are obtained from the corresponding K_j, L_j, M_j and N_j by making the following substitution:

$$\ell_1, m_1, n_1 \rightarrow \ell_2, m_2, n_2;$$

$$\ell_2, m_2, n_2 \rightarrow -\ell_1, -m_1, -n_1; \qquad \varepsilon \leftrightarrow \mu.$$

The interrelationships between various elliptic integrals given above enable us to calculate all of the integrals I, I_a, ... in terms of only two of them for the case of an ellipsoid, and only one of them for the case of a spheroid. These relations are [2]:

$$I_a + I_b + I_c = \frac{2}{abc}$$

$$a^2 I_a + b^2 I_b + c^2 I_c = I$$

$$I_{ab} = (I_a - I_b)/(b^2 - a^2)$$

$$3I_{aa} + I_{ab} + I_{ac} = \frac{2}{a^3 bc}$$

$$3a^2 I_{aa} + b^2 I_{ab} + c^2 I_{ac} = 3I_a \ .$$

APPENDIX B

PROLATE SPHEROIDAL MODEL - EXPRESSIONS FOR COEFFICIENTS

CASE 1

Broadside Incidence — Electric Field Along the Major Axis

In this case, the direction cosines are $n_1 = \ell_2 = m = 1$ and $\ell_1 = m_1 = m_2 = n_2 = \ell = n = 0$. Then the coefficients are:

$$K_3 = \frac{2}{3}(\varepsilon - 1)f_3(\varepsilon)$$

$$15L_3 = f_3(\varepsilon)[(\varepsilon - 1)\frac{6c^2 - 5b^2}{3} - \varepsilon b^2] + f_3(\varepsilon)^2\{(\varepsilon - 1)[(\varepsilon - 2)I$$

$$+ \varepsilon c^2 I_c - \frac{4c}{b^2}] + \frac{2\varepsilon^2}{c}\}$$

$$15N_1 = g_1(\varepsilon)[\varepsilon\frac{b^2 + c^2}{2} - b^2] + f_1(\mu)g_1(\varepsilon)[\varepsilon\frac{b^2 - c^2}{b^2c}]$$

$$15\overline{L}_1 = b^2 f_1(\mu) + f_1^2(\mu)\varepsilon\frac{b^2 + c^2}{b^2c} + f_1(\mu)g_1(\varepsilon)[(I_b - I_c)(b^2 - \varepsilon\frac{b^2 + c^2}{2})$$

$$+ \varepsilon\frac{b^2 - c^2}{b^2c}] + f_1^2(\mu)g_1(\varepsilon)(I_b - I_c)[\varepsilon(\varepsilon - 2)\frac{b^2 - c^2}{b^2c}]$$

$$K_1 = K_2 = L_1 = L_2 = M_1 = M_2 = M_3 = N_2 = N_3 = 0$$

and

$$\overline{K}_1 = \overline{K}_2 = \overline{K}_3 = \overline{L}_2 = \overline{L}_3 = \overline{M}_1 = \overline{M}_2 = \overline{M}_3 = \overline{N}_1 = \overline{N}_2 = \overline{N}_3 = 0.$$

CASE 2

Broadside Incidence — Magnetic Field Along the Major Axis

In this case the direction cosines are: $\ell_1 = -n_2 = m = 1$ and $m_1 = n_1 = \ell_2 = m_2 = \ell = n = 0$; and the expression coefficients are:

$$K_1 = \frac{2}{3}(\varepsilon - 1)f_1(\varepsilon).$$

$$15L_1 = f_1(\varepsilon)\{(\varepsilon - 1)\left(\frac{2b^2 - c^2}{3}\right) - \varepsilon b^2\} + f_1^{\,2}(\varepsilon)\{(\varepsilon - 1)[(\varepsilon - 2)I$$

$$+ \varepsilon b^2 I_a - \frac{4}{c} + \varepsilon^2 \frac{b^2 + c^2}{b^2 c}\} + f_1(\varepsilon)g_1(\mu)[(I_c - I_b)\frac{c^2 - b^2}{2} - \varepsilon\frac{c^2 - b^2}{b^2 c}]$$

$$+ f_1(\varepsilon)^2 g_1(\mu)(I_b - I_c)[(\varepsilon - 1)K_1(\mu) - \varepsilon(\varepsilon - 2)\frac{c^2 - b^2}{b^2 c}].$$

$$15N_3 = g_3(\varepsilon)b^2(\varepsilon - 1).$$

$$15\overline{L}_3 = b^2 f_3(\mu) - 2f_3^{\,2}(\mu)\frac{\varepsilon}{c}.$$

$$15\overline{N}_1 = f_1(\varepsilon)(1 - \varepsilon)\frac{c^2 - b^2}{3} - g_1(\mu)\frac{c^2 - b^2}{2} + f_1(\varepsilon)g_1(\mu)[\varepsilon\frac{c^2 - b^2}{b^2 c}$$

$$+ (\varepsilon - 1)K_1(\mu)].$$

$$K_2 = K_3 = L_2 = L_3 = M_1 = M_2 = M_3 = N_1 = N_2 = 0.$$

$$\overline{K}_1 = \overline{K}_2 = \overline{K}_3 = \overline{L}_1 = \overline{L}_2 = \overline{M}_1 = \overline{M}_2 = \overline{M}_3 = \overline{N}_2 = \overline{N}_3 = 0.$$

CASE 3

Nose-On Incidence

For this case, $\ell_1 = m_2 = n = 1$ and $m_1 = n_1 = \ell_2 = n_2 = \ell = m = 0$. Then the coefficients are given by:

$$K_1 = \frac{2}{3}(\varepsilon - 1)f_1(\varepsilon).$$

$$15L_1 = f_1(\varepsilon)\{(\varepsilon - 1)(\frac{5b^2 - 4c^2}{3}) - \varepsilon c^2\} + f_1(\varepsilon)^2\{(\varepsilon - 1)[(\varepsilon - 2)I$$

$$+ \varepsilon b^2 I_a - \frac{4}{c}] + \varepsilon^2 \frac{b^2 + c^2}{b^2 c}\} + f_1(\varepsilon)g_1(\mu)[I_c - I_b)\frac{c^2 - b^2}{2} + \varepsilon\frac{c^2 - b^2}{b^2 c}]$$

$$+ f_1^2(\varepsilon)g_1(\mu)(I_b - I_c)[(\varepsilon - 1)K_1(\mu) - \varepsilon(\varepsilon - 2)\frac{c^2 - b^2}{b^2 c}].$$

$$15\overline{L}_2 = -f_2(\mu)c^2 + f_2(\mu)^2\varepsilon\frac{b^2 + c^2}{b^2 c} + f_2(\mu)g_2(\varepsilon)[(I_b - I_c)(\varepsilon\frac{b^2 + c^2}{2} - c^2)$$

$$+ \varepsilon\frac{c^2 - b^2}{b^2 c}] + f_2^2(\mu)g_2(\varepsilon)(I_c - I_b)[\varepsilon(\varepsilon - 2)\frac{c^2 - b^2}{b^2 c}].$$

$$15\overline{N}_1 = f_1(\varepsilon)(1 - \varepsilon)\frac{c^2 - b^2}{3} - g_1(\mu)\frac{c^2 - b^2}{2} + f_1(\varepsilon)g_1(\mu)[\varepsilon\frac{c^2 - b^2}{b^2 c}$$

$$+ (\varepsilon - 1)K_1(\mu)].$$

$$K_2 = K_3 = L_2 = L_3 = M_1 = M_2 = M_3 = N_1 = N_2 = N_3 = 0.$$

$$\overline{K}_1 = \overline{K}_2 = \overline{K}_3 = \overline{L}_1 = \overline{L}_3 = \overline{M}_1 = \overline{M}_2 = \overline{M}_3 = \overline{N}_2 = \overline{N}_3 = 0.$$

APPENDIX C

EXTENDED BOUNDARY CONDITION METHOD

C-1. THEORETICAL FORMULATION

Following the procedure given by Barber and Yeh [18] as outlined earlier in the text, the surface currents for external fields (Figure C-1) are given as:

$$\vec{J}_+ = \hat{n} \times (\vec{H}^i + \vec{H}^s) = \hat{n} \times \vec{H}_+$$

and

$$\vec{M}_+ = (\vec{E}^i + \vec{E}^s) \times \hat{n} = \vec{E}_+ \times \hat{n} \ .$$

The scattered fields everywhere due to $\vec{J}_+$ and $\vec{M}_+$ can be determined from the vector potentials of $\vec{A}$ and $\vec{F}$.

$$\vec{A} = \frac{1}{4\pi}\int_s \frac{\vec{J}_+ \exp(jk|\vec{r}-\vec{r}\,'|)}{|\vec{r}-\vec{r}\,'|}\, ds, \qquad \vec{J}_+ = \hat{n} \times \vec{H}_+ \tag{C-1a}$$

and

$$\vec{F} = \frac{1}{4\pi}\int_s \frac{\vec{M}_+ \exp(jk|\vec{r}-\vec{r}\,'|)}{|\vec{r}-\vec{r}\,'|}\, ds, \qquad \vec{M}_+ = \vec{E}_+ \times \hat{n} \tag{C-1b}$$

where $\vec{r}$ and $\vec{r}\,'$ are position vectors from an interior origin to the field and source points, respectively, and $e^{j\omega t}$ time variation has been assumed. Then,

$$\vec{E}^s = -\nabla x \vec{F} - \frac{1}{j\omega\varepsilon_o}(\nabla x \nabla x \vec{A}), \tag{C-2a}$$

$$\vec{N}^s = \nabla x \vec{A} - \frac{1}{j\omega\mu_o}(\nabla x \nabla x \vec{F}). \tag{C-2b}$$

Substituting equations (C-1a) and (C-1b) into equations (C-2a) gives:

$$\vec{E}^s(r) = \nabla x \int_s (\hat{n} X \vec{E}_+) g(kr) ds - \nabla x \nabla x \int_s \frac{1}{j\omega\varepsilon_o} (\hat{n} X \vec{H}_+) g(kr) ds, \tag{C-3}$$

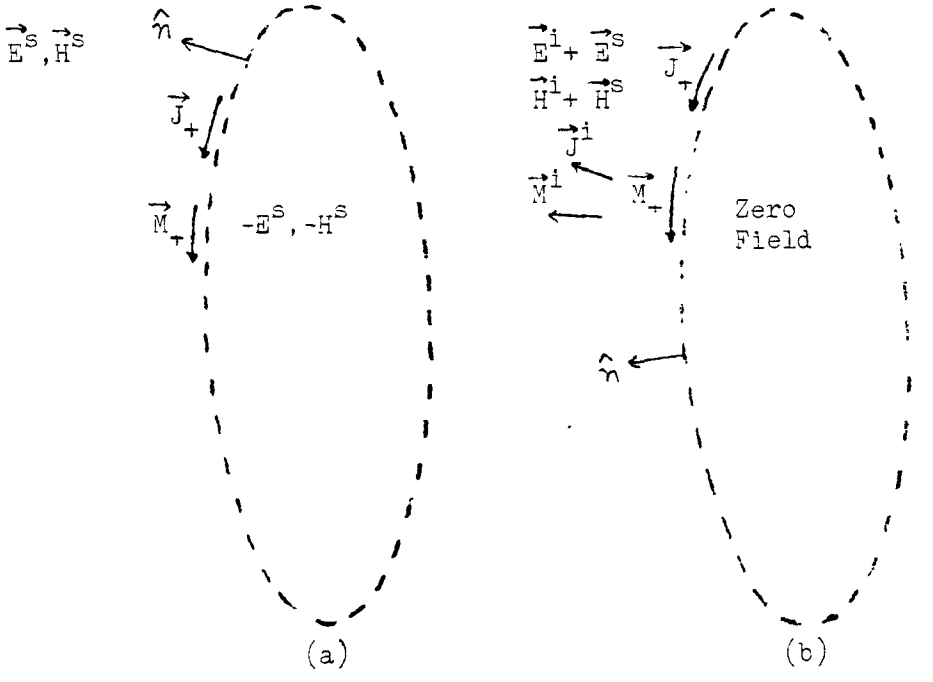

Figure C-1 Summing of Sources and Fields to obtain the external problem.

where g(kr) is the free space Green's function as given by:

$$g(kr) = \exp(jkr)/4\pi r \text{ with } r = |\vec{r}-\vec{r}|, \text{ and } k = 2\pi/\lambda = \omega\sqrt{\mu_o\varepsilon_o} \quad .$$

Then from Figure (C-1b), the total field is given by:

$$\vec{E}^i(\vec{r}) + \vec{E}^s(\vec{r}) = \vec{E}^i(\vec{r}) + \nabla X \int_s (\hat{n}X\vec{E}_+)g(kr)ds - \nabla X\nabla X \int_s \frac{1}{j\omega\varepsilon_o} (\hat{n}X\vec{H}_+)g(kr)ds$$

$$= \begin{cases} \vec{E}(r) & \text{for } \vec{r} \text{ outside s} \\ 0 & \text{for } \vec{r} \text{ inside s} \end{cases} \qquad \text{(C-4)}$$

Thus, for $\vec{r}$ inside s, equation (C-4) determines the surface currents because of the condition that the scattered field cancels the incident field throughout the interior volume, i.e., for $\vec{r}$ inside s,

$$\nabla X \int_s (\hat{n}X\vec{E}_+)g(kr)ds - \nabla X\nabla X \int_s \frac{1}{j\omega\varepsilon_o} (\hat{n}X\vec{H}_+)g(kr)ds = -\vec{E}^i(r). \qquad \text{(C-5)}$$

This equation is expanded by making use of the spherical vector wave functions $\vec{M}$ and $\vec{N}$ which have been defined by Stratton [25]. As a matter of convenience, we have chosen to use complex linear combinations of the even and odd spherical vector wave functions. (The advantages in using complex spherical vector rotation are: i) programming work is more convenient and ii) it reduces the integration computation by half.)

$$\vec{M}_{mn} = \vec{M}_{emn} + j\vec{M}_{omn}$$

$$\vec{N}_{mn} = \vec{N}_{emn} + j\vec{N}_{omn}$$

$$\vec{M}_{mn}(kr) = z_n(kr)e^{jm\phi} \left[\frac{jm}{\sin\theta} P_n^{|m|}(\cos\theta)\hat{e}_\theta - \frac{dP_n^{|m|}(\cos\theta)}{d\theta} \hat{e}_\phi \right] \qquad \text{(C-6a)}$$

and

$$\vec{N}_{mn}(kr) = e^{jm\phi} \{n(n+1) \frac{z_n(kr)}{kr} P_n^{|m|}(\cos\theta)\hat{e}_r + [\frac{z_n(kr)}{kr} + z'_n(kr)]$$

$$X[\frac{dP_n^{|m|}(\cos\theta)}{d\theta} \hat{e}_\theta + \frac{jm}{\sin\theta} P_n^{|m|}(\cos\theta)\hat{e}_\phi]\} \quad . \qquad \text{(C-6b)}$$

and $$\vec{N} = \frac{1}{\kappa} \nabla X \vec{M}, \quad \vec{M} = \frac{1}{\kappa} \nabla X \vec{N}.$$

Here, z_n denotes a spherical Bessel function of order n and $P_n^{|m|}$ denotes the associated Legendre functions of the first kind of degree n and order $|m|$ where m is a positive or negative integer, and n is an integer with $n \geq |m|$ and $n \neq 0$.

For solutions of the wave equation that must be finite at $\vec{r} = 0$, $z_n(kr) = j_n(kr)$, and the resulting vector spherical functions $\vec{M}$ and $\vec{N}$ are known as solutions of the first kind. The other vector spherical functions we will be using are called spherical Hankel functions, $z_n(kr) = h_n^{(1)}(kr) = j_n(kr) + jn_n(kr)$. This solution represents outgoing waves and is called the solution of the third kind.

Using these spherical vector functions, the incident fields are given by:

$$\vec{E}^i(\vec{r}) = \sum_{m=-\infty}^{\infty} \sum_{\substack{n \geq |m| \\ n \neq 0}} D_{mn}[A_{mn}\vec{M}^1_{mn}(k\vec{r}) + B_{mn}\vec{N}^1_{mn}(k\vec{r})] \tag{C-7a}$$

$$\vec{H}^i(\vec{r}) = \frac{jk}{\omega\mu_o} \sum_{m=-\infty}^{\infty} \sum_{\substack{n \geq |m| \\ n \neq 0}} D_{mn}[A_{mn}\vec{N}^1_{mn}(k\vec{r}) + B_{mn}\vec{M}^1_{mn}(k\vec{r})], \tag{C-7b}$$

where D_{mn} is a normalization constant, and the expansion coefficients A_{mn} and B_{mn} are known for a specific incident field. Note that,

$$D_{mn} = \frac{(2n+1)(n-|m|)!}{n(n+1)(n+|m|)!} .$$

The terms in the integrals of equation (C-5) are expanded as follows, with the help of the free space Green's dyadic given by Morse and Feshbaach [26].

$$(\hat{n}X\vec{E}_+)g(kr) = (\hat{n}X\vec{E}_+) \cdot \overline{\overline{G}} \tag{C-8a}$$

$$(\hat{n}X\vec{H}_+)g(kr) = (\hat{n}X\vec{H}_+) \cdot \overline{\overline{G}} \tag{C-8b}$$

The free space Green's dyadic is:

$$\overline{\overline{G}}(k|\vec{r}-\vec{r}'|) = \tilde{I}\left(\frac{\exp jk|\vec{r}-\vec{r}'|}{4\pi|r-r'|}\right) = \frac{jk}{4\pi} \sum_{m=-\infty}^{\infty} \sum_{\substack{n \geq |m| \\ n \neq 0}} D_{mn}[\vec{M}^3_{-mn}(k\vec{r}_>)\vec{M}^1_{mn}(k\vec{r}_<)$$

$$+ \vec{N}^3_{-mn}(k\vec{r}_>)\vec{N}^1_{mn}(k\vec{r}_<) + \text{irrotational terms}] \tag{C-9a}$$

or $$= \frac{jk}{4\pi} \sum_{m=-\infty}^{\infty} \sum_{\substack{n \geq |m| \\ n \neq 0}} D_{mn} [\vec{M}^3_{mn}(k\vec{r}_>)\vec{M}^1_{-mn}(k\vec{r}_<)$$

$$+ \vec{N}^3_{mn}(k\vec{r}_>)\vec{N}^1_{mn}(k\vec{r}_<) + \text{irrotational terms}], \qquad \text{(C-9b)}$$

where $\vec{r}_>$, $\vec{r}_<$ are, respectively, the greater and lesser of $\vec{r}$, $\vec{r}'$. The irrotational terms present in equation (C-9) are washed out due to the curl operation.

Equation (C-5) is required to hold throughout the entire interior volume, i.e., inside s (analytic continuation property). Then, restricting the field point $\vec{r}$ to lie within s,

$$\nabla X \int_s (\hat{n}X\vec{E}_+)g(k\vec{r})ds = \nabla X \int_s (\hat{n}X\vec{E}_+) \cdot \bar{\bar{G}}\, ds$$

$$= \frac{jk}{4\pi} \sum_{m=-\infty}^{\infty} \sum_{\substack{n \geq |m| \\ n \neq 0}} D_{mn} [\int_s (\hat{n}X\vec{E}_+) \cdot [\vec{M}^3_{-mn}(k\vec{r}') \cdot \nabla X \vec{M}^1_{mn}(k\vec{r})$$

$$+ \vec{N}^3_{-mn}(k\vec{r}') \cdot \nabla X \vec{N}^1_{mn}(k\vec{r})]ds]$$

$$= \frac{jk^2}{4\pi} \sum_{m=-\infty}^{\infty} \sum_{\substack{n \geq |m| \\ n \neq 0}} D_{mn} [\int_s (\hat{n}X\vec{E}_+) \cdot (\vec{M}^3_{-mn}(k\vec{r}') \cdot N^1_{mn}(k\vec{r})$$

$$+ \vec{N}^3_{-mn}(k\vec{r}') \cdot \vec{M}^1_{mn}(k\vec{r}))ds].$$

Similarly,

$$\nabla X \nabla X \int_s \frac{1}{j\omega\varepsilon_o} (\hat{n}X\vec{H}_+)g(kr)ds = \frac{jk^2}{4\pi} (-j\sqrt{\frac{\mu_o}{\varepsilon_o}}) \sum_{m=-\infty}^{\infty} \sum_{\substack{n \geq |m| \\ n \neq 0}} D_{mn} [\int_s (\hat{n}X\vec{H}_+)$$

$$\cdot (\vec{M}^3_{-mn}(k\vec{r}') \cdot \vec{M}^1_{mn}(k\vec{r}) + \vec{N}^3_{-mn}(k\vec{r}') \cdot \vec{N}^1_{mn}(k\vec{r})ds].$$

Equation (C-5) becomes:

$$\frac{jk^2}{4\pi} \Sigma\Sigma\, D_{mn} \{\int_s \{[(\hat{n}X\vec{E}_+) \cdot \vec{N}^3_{-mn}(k\vec{r}') + j\sqrt{\frac{\mu_o}{\varepsilon_o}} (\hat{n}X\vec{H}_+) \cdot \vec{M}^3_{-mn}(k\vec{r}')]\vec{M}^1_{mn}(k\vec{r})$$

$$+ [(\hat{n}X\vec{E}_+)\cdot\vec{M}^3_{-mn}(k\vec{r}') + j\sqrt{\frac{\mu_o}{\varepsilon_o}}\ (\hat{n}X\vec{H}_+)\cdot\vec{N}^3_{-mn}(k\vec{r}')]\vec{N}^1_{mn}(k\vec{r})\}ds$$

$$= -\vec{E}^i(k\vec{r})$$

$$= +\Sigma\Sigma D_{mn}[A_{mn}\vec{M}^1_{mn}(k\vec{r}) + B_{mn}\vec{N}^1_{mn}(k\vec{r})] \ . \qquad \text{(C-10)}$$

This gives the following set of equations, because of the orthogonality of the functions over a spherical surface about the origin (or just from the fact that left side and right side are equal if and only if the coefficients corresponding to the same $\vec{M}^1_{mn}$ or $\vec{N}^1_{mn}$ are the same).

$$\frac{jk^2}{4\pi}\int_s[\vec{N}^3_{-mn}(k\vec{r}')\cdot(\hat{n}X\vec{E}_+) + j\sqrt{\frac{\mu_o}{\varepsilon_o}}\ \vec{M}^3_{-mn}(k\vec{r}')\cdot(\hat{n}X\vec{H}_+)]ds = A_{mn} \qquad \text{(C-11a)}$$

$$\frac{jk^2}{4\pi}\int_s[\vec{M}^3_{-mn}(k\vec{r}')\cdot(\hat{n}X\vec{E}_+) + j\sqrt{\frac{\mu_o}{\varepsilon_o}}\ \vec{N}^3_{-mn}(k\vec{r}')\cdot(\hat{n}X\vec{H}_+)]ds = B_{mn} \qquad \text{(C-11b)}$$

The solution of this equation guarantees that the total field will be zero within the inscribed sphere, and hence by using the concept of analytic continuation within the entire interior volume under consideration.

C-2. EXTENDED BOUNDARY CONDITION APPLIED TO THE SURFACE

Now the field inside the lossy dielectric can be approximated by:

$$\vec{E}^t(k'\vec{r}) = -\sum_{m=-\infty}^{\infty}\ \sum_{\substack{n\geq|m|\\ n\neq 0}}[c_{mn}\vec{M}^1_{mn}(k'\vec{r}) + d_{mn}\vec{N}^1_{mn}(k'\vec{r})] \qquad \text{(C-12a)}$$

$$\vec{H}^t(k\vec{r}) = j\frac{k'}{\omega\mu_o}\sum_{m=-\infty}\ \sum_{\substack{n\geq|m|\\ n\neq 0}}[c_{mn}\vec{N}^1_{mn}(k'\vec{r}) + d_{mn}\vec{M}^1_{mn}(k'\vec{r})] \qquad \text{(C-12b)}$$

where $k' = \omega\sqrt{\mu\varepsilon}$.

The boundary condition at the surface requires that the tangential components of the fields be continuous, i.e.,

$$\hat{n}X\vec{H}_+ = \hat{n}X\vec{H}_- \qquad \text{(C-13a)}$$

$$\hat{n}X\vec{E}_+ = \hat{n}X\vec{E}_- \qquad \text{(C-13b)}$$

The (+) and (-) sign subscripts on the surface fields indicate that these fields are the external and internal fields, respectively, at the surface. From equation (C-13), the tangential components of the internal fields at the surface are:

$$\hat{n}X\vec{E}_- = \sum_{m=-\infty}^{\infty} \sum_{\substack{n \geq |m| \\ n \neq 0}} [(c_{mn}\hat{n}X\vec{M}_{mn}(k'\vec{r}') + d_{mn}\hat{n}X\vec{N}_{mn}(k'\vec{r}')] \tag{C-14a}$$

$$\hat{n}X\vec{H}_- = j\frac{k'}{\omega\mu_o} \sum_{m=-\infty}^{\infty} \sum_{\substack{n \geq |m| \\ n \neq 0}} [c_{mn}\hat{n}X\vec{N}_{mn}(k'\vec{r}') + d_{mn}\hat{n}X\vec{M}_{mn}(k'\vec{r}')] \tag{C-14b}$$

Now, due to the equality of the tangential surface fields in equations (C-13), equations (C-14) can be substituted into equations (C-11). Then equation (C-11a) leads to:

$$\frac{jk^2}{4\pi} \sum_{m=-\infty}^{\infty} \sum_{\substack{n' \geq |m| \\ n \neq 0}} \{[\int_s \vec{N}^3_{-mn}(k\vec{r}')X\vec{M}^1_{m'n'}(k'\vec{r}')\cdot\hat{n}ds + \sqrt{\frac{\varepsilon_r}{\mu_r}}\int_s \vec{M}^3_{-mn}(k\vec{r}')X\vec{M}^1_{m'n'}(k'\vec{r}')$$

$$\cdot\hat{n}ds]C_{m'n'} + [\int_s \vec{N}^3_{-mn}(k\vec{r}')X\vec{N}^1_{m'n'}(k'\vec{r}')\cdot\hat{n}ds + \sqrt{\frac{\varepsilon_r}{\mu_r}}\int_s \vec{M}^3_{-mn}(k\vec{r}')X\vec{M}^1_{m'n'}(k'\vec{r}')$$

$$\cdot\hat{n}ds]d_{m'n'} = A_{mn} \tag{C-15a}$$

Similarly,

$$\frac{jk^2}{4\pi} \sum_{m'=-\infty}^{\infty} \sum_{\substack{n \geq |m| \\ n \neq 0}} \{[\int_s \vec{M}_{-mn}(k\vec{r}')X\vec{N}^1_{m'n'}(k'\vec{r}')\cdot\hat{n}ds + \sqrt{\frac{\varepsilon_r}{\mu_r}}\int_s \vec{N}_{-mn}(k\vec{r}')X\vec{M}^1_{m'n'}(k'\vec{r}')$$

$$\cdot\hat{n}ds]C_{m'n'}\} + [\int_s \vec{M}^3_{-mn}(k\vec{r}')X\vec{M}^1_{m'n'}(k'\vec{r}')\cdot\hat{n}ds + \sqrt{\frac{\varepsilon_r}{\mu_r}}\int_s \vec{N}^3_{-mn}(k\vec{r}')X\vec{N}^1_{m'n'}(k'\vec{r}')$$

$$\cdot\hat{n}ds]d_{m'n'} = B_{mn} \tag{C-15b}$$

$$m = -\infty \text{ to } \infty \qquad n \geq |m|,\ n \neq 0$$

$$n' = -\infty \text{ to } \infty \qquad n' \geq |m|,\ n \neq 0$$

Using the notations:

$$I_{mm'nn'} \triangleq \frac{k^2}{4\pi} \int_s \hat{n}\cdot\vec{M}^3_{-mn}(k\vec{r}')\times\vec{M}^1_{m'n'}(k'\vec{r}')ds$$

$$J_{mm'nn'} \triangleq \frac{k^2}{4\pi} \int_s \hat{n}\cdot\vec{M}^3_{-mn}(k\vec{r}')\times\vec{N}^1_{m'n'}(k'\vec{r}')ds$$

$$K_{mm'nn'} \triangleq \frac{k^2}{4\pi} \int_s \hat{n}\cdot\vec{N}^3_{-mn}(k\vec{r}')\times\vec{M}^1_{m'n'}(k'\vec{r}')ds$$

$$K_{mm'nn'} \triangleq \frac{k^2}{4\pi} \int_s \hat{n}\cdot\vec{N}^3_{-mn}(k\vec{r}')\times\vec{N}^1_{m'n'}(k'\vec{r}')ds$$

leads to:

$$\sum_{m',n'} \{[K + \sqrt{\frac{\varepsilon_r}{\mu_r}}\, J]c_{m'n'} + [L + \sqrt{\frac{\varepsilon_r}{\mu_r}}\, I]d_{m'n'} = -jA_{mn} \qquad \text{(C-16a)}$$

$$\sum_{m',n'} [I + \sqrt{\frac{\varepsilon_r}{\mu_r}}\, L]c_{m'n'} + [L + \sqrt{\frac{\varepsilon_r}{\mu_r}}\, I]d_{m'n'} = -jB_{mn} \qquad \text{(C-16b)}$$

These are infinite sets of linear equations and can be approximately solved for c's and d's by truncating and utilizing suitable numerical methods.

Subsequent similar analysis provides a relationship between these coefficients and the expansion coefficients of the scattered field. Scattered fields are assumed to be expanded as follows.

$$\vec{E}^s(k\vec{r}) = -\sum_{m=-\infty}^{\infty} \sum_{\substack{n\geq|m| \\ n\neq 0}} D_{mn}[a_{mn}\vec{M}^3_{mn}(k\vec{r}) + b_{mn}\vec{N}^3_{mn}(k\vec{r})], \qquad \text{(C-17a)}$$

and

$$\vec{H}^s(kr) = \frac{jk}{\omega\mu_o} \sum_{m=-\infty}^{\infty} \sum_{\substack{n\geq|m| \\ n\neq 0}} D_{mn}[a_{mn}\vec{N}^3_{mn}(k\vec{r}) + b_{mn}\vec{M}^3_{mn}(k\vec{r})] \qquad \text{(C-17b)}$$

Following as in previous case leads to:

$$ja_{mn} = \sum_{m'} \sum_{n'} \{[K' + \sqrt{\frac{\varepsilon_r}{\mu_r}}\, J']c_{m'n'} + [L' + \sqrt{\frac{\varepsilon_r}{\mu_r}}\, I']d_{m'n'}\} \qquad \text{(C-18a)}$$

$$jb_{mn} = \sum_{m'} \sum_{n'} \{[I' + \sqrt{\frac{\varepsilon_r}{\mu_r}} L']c_{m'n'} + [J' + \sqrt{\frac{\varepsilon_r}{\mu_r}} K']d_{m'n'} \tag{C-18b}$$

where

$$I'_{mm'nn'} \triangleq \frac{k^2}{4\pi} \int_s \hat{n}\cdot\vec{M}^1_{-mn}(k\vec{r}')X\vec{M}^1_{m'n'}(k'\vec{r}')ds$$

$$J'_{mm'nn'} \triangleq \frac{k^2}{4\pi} \int_s \hat{n}\cdot\vec{M}^1_{-mn}(k\vec{r}')X\vec{N}^1_{m'n'}(k'\vec{r}')ds$$

$$K_{mm'nn'} \triangleq \frac{k^2}{4\pi} \int_s \hat{n}\cdot\vec{N}^1_{-mn}(k\vec{r}')X\vec{M}^1_{m'n'}(k'\vec{r}')ds$$

$$L_{mm'nn'} \triangleq \frac{k^2}{4\pi} \int_s \hat{n}\cdot\vec{N}^1_{-mn}(k\vec{r}')X\vec{N}^1_{m'n'}(k'\vec{r}')ds$$

From (C-16) and (C-18), a_{mn} and b_{mn} can be expressed in terms of A_{mn} and B_{mn} by using matrix notation.

$$\begin{bmatrix} a_{mn} \\ b_{mn} \end{bmatrix} = \begin{bmatrix} K'+\sqrt{\frac{\varepsilon_r}{\mu_r}} J' & L'+\sqrt{\frac{\varepsilon_r}{\mu_r}} I' \\ I'+\sqrt{\frac{\varepsilon_r}{\mu_r}} L' & J'+\sqrt{\frac{\varepsilon_r}{\mu_r}} K' \end{bmatrix} \begin{bmatrix} K+\sqrt{\frac{\varepsilon_r}{\mu_r}} J & L+\sqrt{\frac{\varepsilon_r}{\mu_r}} I \\ I+\sqrt{\frac{\varepsilon_r}{\mu_r}} L & J+\sqrt{\frac{\varepsilon_r}{\mu_r}} K \end{bmatrix}^{-1} \begin{bmatrix} -A_{mn} \\ -B_{mn} \end{bmatrix} \tag{C-19}$$

C-3. APPLICATION TO SPHEROIDAL PROBLEM

Due to the axial symmetry property, the integration from $\phi = 0$ to $\phi = 2\pi$ gives the complete orthogonality property, i.e., the terms with $m' \neq m$ vanish. Then since,

$$\hat{n}ds = (\hat{e}_r - \frac{dr}{rd\theta}\hat{e}_\theta)r^2 \sin\theta d\theta d\phi$$

$$I_{mnn'} = \frac{k^2}{4\pi}\int_s \hat{n}\cdot\vec{M}^3_{-mn}(k\vec{r}')X\vec{M}^1_{mn}(k'\vec{r}')ds$$

$$= \frac{jm}{2}\int_0^\pi [h^1_n(kr)j_{n'}(k'r)(P^m_n(\cos\theta)\frac{dP^m_{n'}}{d\theta}(\cos\theta) + \frac{dP^m_n}{d\theta}(\cos\theta)P^m_{n'}(\cos\theta)] \tag{C-20a}$$

Similarly,

$$J_{mnn'} = \frac{1}{2}\int_0^{\pi} [h_n^1(kr)(\frac{j_{n'}(k'r)}{k'r} + j_{n'}'(k'r))(\frac{m^2}{\sin^2\theta} P_n^m(\cos\theta)P_{n'}^m(\cos\theta)$$

$$+ \frac{dP_n^m(\cos\theta)}{d\theta}\frac{dP_{n'}^m(\cos\theta)}{d\theta}) + n'(n'+1)h_n^1(kr)\frac{j_{n'}(k'r)}{k'r}\frac{dP_n^m(\cos\theta)}{d\theta} P_{n'}^m(\cos\theta)$$

$$(\frac{dr}{rd\theta})](kr)^2\sin\theta d\theta \qquad \text{(C-20b)}$$

$$K_{mnn'} = \frac{-1}{2}\int_0^{\pi}\{[\frac{h_n^1(kr)}{kr} + h_n^{1\prime}(kr)]j_{n'}(k'r)(\frac{m^2}{\sin^2\theta} P_n^m(\cos\theta)P_{n'}^m(\cos\theta)$$

$$+ \frac{dP_n^m(\cos\theta)}{d\theta}\frac{dP_{n'}^m(\cos\theta)}{d\theta}) + n(n+1)\frac{h_n^1(kr)}{kr} j_{n'}(k'r)P_n^m(\cos\theta)$$

$$\cdot \frac{dP_{n'}^m(\cos\theta)}{d\theta}(\frac{dr}{rd\theta})\}(kr)^2\sin\theta d\theta \qquad \text{(C-20c)}$$

$$L_{mnn'} = j\frac{m}{2}\int_0^{\pi}\{[\frac{h_n^1(kr)}{kr} + h_n^{1\prime}(kr)][\frac{j_{n'}(k'r)}{k'r} + j_{n'}'(k'r)](P_n^m(\cos\theta)\frac{dP_{n'}^m(\cos\theta)}{d\theta}$$

$$+ P_{n'}^m(\cos\theta)\frac{dP_n^m(\cos\theta)}{d\theta}) + P_n^m(\cos\theta)P_{n'}^m(\cos\theta)[n(n+1)\frac{h_n^1(kr)}{kr}$$

$$[\frac{j_{n'}(k'r)}{k'r} + j_{n'}'(k'r)] + n'(n'+1)(\frac{h_n'(kr)}{kr} + h_n^{1\prime}(kr))\frac{j_{n'}(k'r)}{k'r}]$$

$$(\frac{dr}{rd\theta})\}(kr)^2 d\theta \qquad \text{(C-20d)}$$

And using the mirror symmetry property of spheroid, $r(\pi - \theta) = r(\theta)$, and with aids of the properties as:

$$\cos(\pi - \theta) = -\cos\theta, \quad \sin(\pi - \theta) = \sin\theta$$

$$P_n^m(\cos(\pi-\theta)) = P_n^m(-\cos\theta) = (-1)^{m+n}P_n^m(\cos\theta)$$

$$\frac{1}{r}\frac{dr}{d\theta} = \frac{(a^2-b^2)\sin\theta\cos\theta}{a^2\cos^2\theta + b^2\sin^2\theta} = \left.\frac{1}{r}\frac{dr}{d\theta}\right|_{\pi-\theta} = -\left.\frac{1}{r}\frac{dr}{d\theta}\right|_{\theta}$$

and

$$\frac{dP_n^m(\cos(\pi-\theta))}{d\theta} = \frac{1}{2}\left[(n-m+1)(n+m)P_n^{m-1}(\cos(\pi-\theta)) - P_n^{m+1}(\cos(\pi-\theta))\right]$$

$$= (-1)^{m+n+1}\frac{dP_n^m(\cos\theta)}{d\theta}$$

leads to:

$$I_{mnn'} = L_{mnn'} = 0 \text{ for } n + n' \text{ even} \tag{C-21a}$$

$$J_{mnn'} = K_{mnn'} = 0 \text{ for } n + n' \text{ odd} \tag{C-21b}$$

and integration is performed from $\theta = 0$ to $\theta = \pi/2$. Equation (C-21) reduces the matrix size further by a factor of two. In addition, our definition of complex spherical wave functions leads to:

For polarization I, (H field parallel to minor axis)

$$a^I_{-mn} = -a^I_{mn} \quad , \quad b^I_{-mn} = b^I_{mn}$$
$$c^I_{-mn} = -c^I_{mn} \quad , \quad d^I_{-mn} = d^I_{mn} \tag{C-22a}$$

For polarization II, (E field parallel to minor axis)

$$a^{II}_{-mn} = a^{II}_{mn} \quad , \quad b^{II}_{-mn} = -b^{II}_{mn}$$
$$c^{II}_{-mn} = c^{II}_{mn} \quad , \quad d^{II}_{-mn} = -d^{II}_{mn} \tag{C-22b}$$

These lead to the following expressions for I, J, K and L.

$$I_{mnn'} = jm\int_0^{\frac{\pi}{2}} h_n'(kr)j_{n'}(k'r)\left[P_n^m(\cos\theta)\frac{dP_{n'}^m(\cos\theta)}{d\theta} + P_{n'}^m(\cos\theta)\frac{dP_n^m(\cos\theta)}{d\theta}\right]$$

$$(kr)^2 d\theta; \text{ for } n + n' \text{ odd} \tag{C-23a}$$

$$J_{mnn'} = \int_0^{\pi/2} \{h_n'(kr)(\frac{j_{n'}(k'r)}{k'r} - j_{n'}'(k'r))[\frac{m^2}{\sin\theta} P_n^m(\cos\theta)P_{n'}^m(\cos\theta)$$

$$+ \frac{dP_n^m(\cos\theta)}{d\theta} \frac{dP_{n'}^m(\cos\theta)}{d\theta}] + n'(n'+1)h_n'(kr) \frac{j_{n'}(k'r)}{k'r} \frac{dP_n^m(\cos\theta)}{d\theta}$$

$$(\frac{dr}{rd\theta})\} (kr)^2 \sin\theta d\theta; \text{ for } n + n' \text{ even} \qquad \text{(C-23b)}$$

$$K_{mnn'} = -\int_0^{\pi/2} \{[\frac{h_n^1(kr)}{kr} + h_n^{1'}(kr)]j_{n'}(k'r)[\frac{m^2}{\sin^2\theta} P_n^m(\cos\theta)P_{n'}^m(\cos\theta)$$

$$+ \frac{dP_n^m(\cos\theta)}{d\theta} \frac{dP_{n'}^m(\cos\theta)}{d\theta}] + n(n+1) \frac{h_n^1(kr)}{kr} j_{n'}(k'r)P_n^m(\cos\theta)$$

$$\frac{dP_{n'}^m(\cos\theta)}{d\theta} (\frac{dr}{rd\theta})\}(kr)^2 \sin\theta d\theta; \text{ for } n + n' \text{ even} \qquad \text{(C-23c)}$$

$$L_{mnn'} = jm\int_0^{\pi/2} \{[\frac{h_n^1(kr)}{kr} + h_n^{1'}(kr)][\frac{j_{n'}(k'r)}{k'r} + j_{n'}'(k'r)][P_n^m(\cos\theta)$$

$$\frac{dP_{n'}^m(\cos\theta)}{d\theta} + \frac{dP_n^m(\cos\theta)}{d\theta} P_{n'}^m(\cos\theta)] + (\frac{dr}{rd\theta})P_n^m(\cos\theta)P_{n'}^m(\cos\theta)$$

$$[n(n+1) \frac{h_n'(kr)}{kr} (\frac{j_{n'}(k'r)}{k'r} + j_{n'}'(k'r)) + n'(n'+1)(\frac{h_n^1(kr)}{kr}$$

$$+ h_n^{1'}(kr)) \frac{j_{n'}(k'r)}{k'r}\}(kr)^2 d\theta.$$

The expressions for $I'_{mnn'}$, $J'_{mnn'}$, $K'_{mnn'}$ and $L'_{mnn'}$ are the same if we replace $h_n^1(kr)$ by $j_n(kr)$.

APPENDIX D

DESCRIPTION OF COMPUTER PROGRAM FOR EBCM

D-1. INTRODUCTION

This program has been written in FORTRAN IV for CDC 6400-CYBER computer. Several factors were given consideration in the design of the program.

Efficient coding was emphasized to reduce the computer run time, and redundant expressions were avoided as much as possible. The complicated expressions are degrouped for the use of other inter-related expressions. This program can be run on any other standard computer with FORTRAN compilers supporting complex variables, with one addition of subroutine for the solution of complex linear equations. In our program, the math-subroutine from IMSL was used for that purpose.

Full single word accuracy of CYBER machine is 14-15 digits, and the double precision for complex variables are not provided, even though for some situation, it was desirable. The memory occupation is not very significant to this program because several (20 x 10) matrices are sufficient to give accurate results as long as the matrix doesn't become ill-conditioned. It was observed that once the matrix becomes ill-conditioned, the increase in matrix size does not contribute to any significant improvement.

D-2. GLOSSARY OF THE SUBROUTINES

The program operated via a main routine and 10 subroutines including one IMSL math routine, which are briefly described and listed below. Standard I/O and mathematical routines; e.g., sin, cos, etc., are assumed to be available.

The main routine, called EBCD, controls overall run processing, and computes [I], [J], [K], and [L] matrices, and the final results of the scattering efficiency, the absorption efficiency and the extinction efficiency.

Subroutine Scatter: computes the contribution to the overall scattering and the extinction of each azimuthal index m.

Subroutine Sphere: computes the scattering and extinction coefficients for the known ideal case of the sphere for comparison and for the program testing for the early stage of this work.

Subroutine Shape: computes the geometrical variables for our model of spheroid.

Subroutine Hankel: computes the spherical Hankel functions of 3rd kind for real arguments.

Subroutine SPHBESS: computes the spherical Bessel functions for complex arguments.

Subroutine Legendr: computes the associated Legendre functions.

Subroutine LEQT2C: (IMSL math-routine) performs the L-U decomposition of complex matrix, and then computes the solution of complex linear equations by iteration method.

Minor Routines

Subroutine MULTRX: computes the multiplication of square matrix with column matrix.

Function DFACT: computes the double factorial defined as (2n)!!

Function FACT: computes the factorial of integer n.

D-3. COMPUTATION OF SPECIAL FUNCTIONS

A. Associated Legendre Functions

Subroutine LEGENDR generates the associated Legendre function $P_n^m(\cos\theta)$, its derivatives $(dP_n^m)/(d\theta)$, and the frequently used $(mP_n^m)/(\sin\theta)$ for a given angle θ, a given value of the azimuthal index m, and for all values of degree n from m to specified n_{max}.

The following recursion relation and formula were used.

$$(2n + 1)\cos\theta P_n^m = (n + m)P_{n-1}^m + (n - m + 1)P_{n+1}^m$$

or

$$P_{n+1}^m = 2\cos\theta P_n^m - P_{n-1}^m + \frac{(2n-1)(\cos\theta P_n^m - P_{n-1}^m)}{n-m+1} \qquad \text{(D-1)}$$

and for the derivatives,

$$\frac{dP_n^m}{d\theta} = \frac{1}{\sin\theta}\left[(n - m + 1)P_{n+1}^m - (n + 1)\cos\theta P_n^m\right] . \qquad \text{(D-2)}$$

Beginning with:

$$P_m^m(\cos\theta) = \frac{(2m)!\sin^m\theta}{2^m m!} \triangleq (2m)!!\sin^m\theta \qquad \text{(D-3)}$$

$$P^m_{m+1}(\cos\theta) = (2m + 1)\cos\theta P^m_m(\cos\theta). \tag{D-4}$$

Special note for $m = 0$, and $\theta = 0°$.

i) For $m = 0$, $\theta = 0°$; $P^0_n = 1$. $\frac{dP^0_n}{d\theta} = 0$. $\frac{mP^0_n}{\sin\theta} = 0$.

ii) For $m = 1$, $\theta = 0°$; $P^m_n = 0$. $\frac{dP^m_n}{d\theta} = \frac{mP^m_n}{\sin\theta} = \frac{n(n+1)}{2}$.

iii) For $m \geq 2$, $\theta = 0°$; $P^m_n = \frac{dP^m_n}{d\theta} = \frac{mP^m_n}{\sin\theta} = 0$.

B. Hankel Functions

Subroutine HANKEL generates the Hankel functions of the third kind, and its derivatives, for a specified real argument x, for all values of order n from 0 to n_{max} specified.

i) Spherical Bessel Functions

The backward recursive relation is used as:

$$j_{n-1}(x) = \frac{2n+1}{x} j_n(x) - j_{n+1}(x), \tag{D-5a}$$

beginning with sufficiently large $N >> n_{max}$, $j_{N+1} = j_N = 0$. Then normalized with respect to $j_0(x) = (\sin x)/x$.

ii) Spherical Neumann Functions

The forward recursive relation is used as:

$$\eta_{n+1}(x) = \frac{2n+1}{x} \eta_n(x) - \eta_{n-1}(x), \tag{D-5b}$$

beginning with $\eta_0(x) = (-\cos x)/x$, and $\eta_1(x) = (\cos x)/(x^2) - (\sin x)/(x)$.

iii) Derivatives in either cases are computed by:

$$f'_n(x) = \frac{nf_{n-1}(x) - (n+1)f_{n+1}(x)}{2n+1} . \tag{D-6}$$

C. Spherical Bessel Functions for Complex Arguments

Subroutine SPHBESS generates the spherical Bessel functions and its derivatives for complex arguments, for a specified argument x and for all the values of n from 0 to n_{max} specified, by the same method as for the real argument.

D-4. COMPUTATION OF GEOMETRICAL FACTORS

Subroutine SHAPE computes r and $(dr)/(rd\theta)$ for a given θ and for a given dimension of a and b, as:

$$r = \frac{ab}{(a^2\cos^2\theta+b^2\sin^2\theta)^{1/2}} \tag{D-7}$$

$$\frac{dr}{rd\theta} = (a^2 - b^2)\cos\theta\sin\theta/(a^2\cos^2\theta + b^2\sin^2\theta)^{1/2}. \tag{D-8}$$

D-5. COMPUTATION OF SCATTERING, ABSORPTION AND EXTINCTION CHARACTERISTICS

$$Q_t \triangleq -\mathrm{Re}[\sum_m \sum_n \frac{n(n+1)(n+|m|!)}{(2n+1)(n-|m|!)} (a_{nm}A^*_{mn} + b_{mn}B^*_{mn})]$$

$$= -\mathrm{Re}[\sum_m \sum_n (-i)^{n-1}\{[a_{mn} \frac{m}{\sin\alpha} P_n^{|m|}(\cos\alpha) + b_{mn} \frac{dP_n^{|m|}(\cos\alpha)}{d\alpha}]\}$$

for electric polarization, and

$$Q_t = -\mathrm{Re}[\sum_m \sum_n (-1)^n[a_{mn} \frac{dP_n^{|m|}(\cos\alpha)}{d\alpha} + b_{mn} \frac{m}{\sin\alpha} P_n^{|m|}(\cos\alpha)] \tag{D-9}$$

for magnetic polarization.

$$Q_s \triangleq \sum_m \sum_n \frac{n(n+1)(n+|m|!)}{(2n+1)(n-|m|!)} (|a_{mn}|^2 + |b_{mn}|^2) \tag{D-10}$$

$$Q_a = Q_t - Q_s . \tag{D-11}$$

Then the cross-sections are computed by:

$$\sigma_t = \frac{4\pi}{k_0^2} Q_t, \ \sigma_s = \frac{4\pi}{k_0^2} Q_s, \ \sigma_a = \frac{4\pi}{k_0^2} Q_a \tag{D-12}$$

and the efficiencies are computed by:

$$\eta_t = \sigma_t/\pi a(a^2\cos^2\alpha + b^2\sin^2\alpha)^{1/2} \tag{D-13}$$

$$\eta_s = \sigma_s/\pi a(a^2\cos^2\alpha + b^2\sin^2\alpha)^{1/2}$$

$$\eta_a = \sigma_a/\pi a(a^2\cos^2\alpha + b^2\sin^2\alpha)^{1/2}.$$

D-6. INTEGRATION SCHEMES

There are various numerical schemes of integration available. Our choice was the simple Trapezoidal rule against other methods. For the periodic function with a continuous k^{th} order derivatives, if the integration is taken over period, then this scheme gives better results than other methods. Though Bode's 6th order scheme was also tested, and the results were the same.

$$\text{Trapezoidal rule; } \int_0^{x_n} f(x)dx = h\left[\frac{f_0}{2} + f_1 + \ldots + f_{n-1} + \frac{f_n}{2}\right] \quad \text{(D-14)}$$

$$\text{Bode's 6th order; } \int_{x_0}^{x_b} f(x)dx = \frac{b}{140}\left[41f_0 + 216f_1 + 27f_2 + 272f_3 + 27f_4 + 216f_5 + 41f_6\right]. \quad \text{(D-15)}$$

D-7. DESCRIPTION OF VARIABLES USED IN THE PROGRAM

Special care was taken to have the variables named as close to its representation in mathematical expressions.

A. Special Function

i) Legendre function:

$$P(n) \triangleq P_n^m(\cos\theta),\ DP(n) \triangleq \frac{dP_n^m(\cos\theta)}{d\theta},\ PM(n) = \frac{mP_n^m(\cos\theta)}{\sin\theta},$$

ii) Hankel function:

$$SPHANK(n) \triangleq h_n(x) = j_n(x) + j\eta_n(x)$$

$$DSPHANK(n) \triangleq h_n'(x) = j_n'(x) - j\eta_n'(x),$$

iii) Spherical Bessel functions for complex argument:

$$\left.\begin{array}{l} SPB(n) \triangleq j_n(x) \\ DSPB(n) \triangleq j_n'(x) \end{array}\right\} ;\ x \text{ complex.}$$

B. Matrices for Surface Integration

$$IMM1(i,k) \triangleq \frac{k^2}{4\pi}\int_S \hat{n} \cdot M_{-m,i}^{(3)}(k\vec{r}') \times M_{m,j}^{(1)}(k_1\vec{r}')ds, \text{ for } i+j \text{ even}$$

$$JMN1(i,k) \triangleq \frac{k^2}{4\pi}\int_s \hat{n} \cdot M^{(3)}_{-m,i}(k\vec{r}') \times N^{(1)}_{m,j}(k_1\vec{r}')ds, \quad \text{for } i+j \text{ odd}$$

$$KMN1(i,k) \triangleq \frac{k^2}{4\pi}\int_s \hat{n} \cdot N^{(3)}_{-m,i}(k\vec{r}') \times M^{(1)}_{m,j}(k_1\vec{r}')ds, \quad \text{for } i+j \text{ odd}$$

$$LMN1(i,k) \triangleq \frac{k^2}{4\pi}\int_s \hat{n} \cdot N^{(3)}_{-m,i}(k\vec{r}') \times N^{(1)}_{m,j}(k_1\vec{r}')ds, \quad \text{for } i+j \text{ even}$$

and IMN2, JMN2, KMN2, LMN2 correspond to $M^{(3)}_{-m,i} \to M^{(1)}_{-m,i}$, $N^{(3)}_{-m,i} \to N^{(1)}_{-m,i}$.

C. <u>Matrices for Linear Equation</u>

i) $$PMTRX1(n,n) = \begin{bmatrix} KJ_{mm} & LI_{m,m+1} & KJ_{m,m+2} & \cdots \\ TL_{m+1,m} & JK_{m+1,m+1} & TL_{m+1,m+2} & \\ KJ_{m+2,m} & LT_{m+2,m+1} & \cdots & \\ \vdots & & & \end{bmatrix}$$

ii) $$QMTRX1(n,n) = \begin{bmatrix} JK_{m,m} & TL_{m,m+1} & JK_{m,m+2} & \cdots \\ LT_{m+1,m} & KJ_{m+1,m+1} & LT_{m+1,m+2} & \cdots \\ JK_{m+2,m} & ZL_{m+2,m+1} & \cdots & \\ \vdots & & & \end{bmatrix}$$

where $KJ_{i,j} \triangleq KMN1(i,k) + \sqrt{\varepsilon_r}\ JMNI(i,k)$ and so on. PMTRX2(n,n) and QMTRX2(n,n) correspond to IMN2, JMN2, KMN2, LMN2. (Note: for m = 0, PMTRX1 and QMTRX1(n,n) interchanges its role.)

iii) WA1(N), WA2(N) $\triangleq$ The first (nxn) locations contain the L-U decomposition of a row-wise permutations of linear matrix. The last n locations contain the pivot indices. The remainder is used as a temporary work space.

WA1, WA2 correspond to PMTRX1, QMTRX1, respectively.

iv) The right-hand side of linear equation:

$$COEFI(n) \text{ for } PMTRX1 \triangleq i^{n+1}\ \frac{m}{\sin\alpha}\ P_n^{|m|}(\cos\alpha) \text{ or } i^{n+1}\ \frac{dP_n^m(\cos\alpha)}{d\alpha}$$

COEF2(n) for QMTRX1

Other are like: X(n), Y(n) are used for temporary input and output of linear equations.

QA(10,2) $\triangleq$ Absorption characteristics

QS(10,2) $\triangleq$ Scattering characteristics

QT(10,2) $\triangleq$ Extinction characteristics

where the first dimension represents the incident angle, and the second dimension represents the polarization mode.

COA(10) = the cosines of incident angle α

SIA(10) = the sines of incident angle α .

D-8. INPUTS TO THE PROGRAM

Card 1; A,B

where A $\triangleq$ the dimension of the long axis of the spheroid in cm.
B $\triangleq$ the dimension of the short axis of the spheroid in cm.

Card 2; FREQ, EPS

where FREQ $\triangleq$ the frequency of the input wave in MHz.
EPS $\triangleq$ the corresponding relative dielectric coefficients of the model (complex).

Card 3; NMAX, MMAX, KMAX, NSECT, KEY

where NMAX $\triangleq$ n_{max}
MMAX $\triangleq$ m_{max}
KMAX $\triangleq$ the number of incident angles considered
NSECT $\triangleq$ the number of integration steps from 0 to $\pi/2$
KEY $\triangleq$ the parameter to be used for printing control of (I,J,K, L) matrix. If K = 0, printing suppressed, if K = 1, print the matrices.

D-9 OUTLINE OF THE GENERAL FLOW OF THE PROGRAM

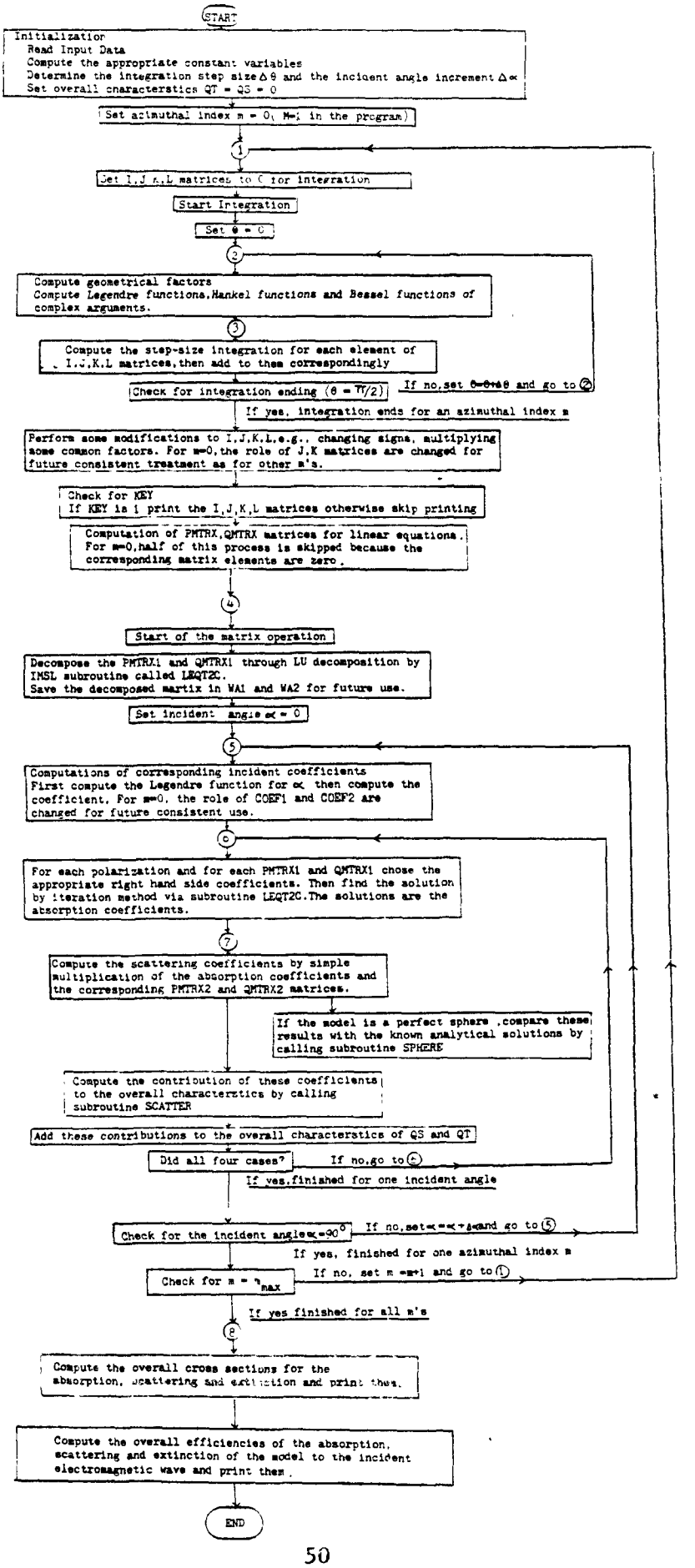

D-10 PROGRAM LISTING

```
      PROGRAM EBCD(INPUT,OUTPUT)
      REAL K0,KB,KPSQ,P(40),DP(40),PM(40),COA(10),SIA(10)
      REAL QA(10,2),QS(10,2),QT(10,2)
      COMPLEX IMG,IMS,EPS,RATIO,K1,RK1,WRK1,BESIJ,WH,WHD,SPH,DSPH,DIJ
      COMPLEX TDIJ,HI,HJ1,HJ2,HK1,HK2,HL1,HL2,HL3,X(20),Y(20),SPHANK(40)
      COMPLEX DSPHANK(40),SPB(100),DSPB(40),COEF1(20),COEF2(20),WA1(460)
      COMPLEX WTEM,WA2(460),IMN1(20,10),JMN1(20,10),KMN1(20,10)
      COMPLEX LMN1(20,10),IMN2(20,10),JMN2(20,10),KMN2(20,10)
      COMPLEX LMN2(20,10),PMTRX1(20,20),PMTRX2(20,20),QMTRX1(20,20)
      COMPLEX QMTRX2(20,20)
      COMMON/BLK1/P,DP,PM/BLK2/SPHANK,DSPHANK/BLK3/SPB,DSPB
      COMMON/BLK4/X/BLK5/ASQ,BSQ,AB,ABQ,K0,K1
      PI=3.1415926535898
      RECT=0.5*PI
      RADIAN=180./PI
      IMG=(0.,1.)
      IMS=(0.,-1.)
      OM=(PI+PI)/2.998E10
      READ 1000,A,B
 1000 FORMAT(2F8.4)
      ASQ=A*A
      BSQ=B*B
      AB=A*B
      ABQ=ASQ-BSQ
      READ 1100, FREQ,EPS
 1100 FORMAT(3F10.4)
      FREQ=FREQ*1.E6
      K0=OM*FREQ
      KB=K0*B
      RATIO=CSQRT(EPS)
      K1=RATIO*K0
      READ 1200, NMAX,MMAX,KMAX,NSECT,KEY
 1200 FORMAT(3I2,I3,I2)
      NHALF=NMAX/2
      NMAX=2*NHALF
      WRITE 2000, A,B,FREQ,EPS,KB,NMAX,MMAX,KMAX,NSECT
 2000 FORMAT(1H1,//////,3X,*A*,F6.2,3X,*B*,F7.2,3X,*FREQ*,E11.4,3X,
     1        *EPS*,2F8.2,3X,*KB*,F7.3,//,3X,*NMAX*,I3,3X,*MMAX*,I3,3X,
     2        *KMAX*,I3,3X,*INTEGRAL SECTION*,I3,///)
      J=KMAX-1
      DTH=RECT/FLOAT(J)
      DAL=DTH*RADIAN
      THETA=0.
      DO 10 I=2,J
      THETA=THETA+DTH
      COA(I)=COS(THETA)
      SIA(I)=SIN(THETA)
   10 CONTINUE
      COA(1)=SIA(KMAX)=1.
      SIA(1)=COA(KMAX)=0.
?
```

```
      DO 20 I=1,20
      QS(I)=QT(I)=0.
   20 CONTINUE
      DTH=RECT/FLOAT(NSECT)
      DO 40 I=1,NMAX
      DO 40 J=1,NMAX
      PMTRX1(J,I)=PMTRX2(J,I)=(0.,0.)
      QMTRX1(J,I)=QMTRX2(J,I)=(0.,0.)
   40 CONTINUE
      DO 700 M=1,MMAX
      DO 120 I=1,NHALF
      DO 120 J=1,NMAX
      IMN1(J,I)=JMN1(J,I)=KMN1(J,I)=LMN1(J,I)=(0.,0.)
      IMN2(J,I)=JMN2(J,I)=KMN2(J,I)=LMN2(J,I)=(0.,0.)
  120 CONTINUE
      MN=M
      IF(M .EQ. 1)MN=2
      THETA=0.
      COSTH=1.
      SINTH=0.
      DO 450 ISECT=1,3
      IF(ISECT-2) 125,130,125
  125 SPMUL=0.5*DTH
      IMAX=1
      GO TO 150
  130 SPMUL=DTH
      IMAX=NSECT-1
  150 DO 400 I=1,IMAX
      CALL SHAPE(COSTH,SINTH,RK0,RK1,RD,WRK0,WRK1,KRSQ)
      CALL HANKEL(RK0,MN,NMAX)
      CALL SPHBESS(RK1,MN,NMAX)
      CALL LEGENDR(COSTH,SINTH,M,MN,NMAX)
      IFLAG=1
      N=MN
      DO 350 MROW=1,NMAX
      IF(IFLAG .EQ. 1) GO TO 160
      NI=MN
      NJ=MN+1
      GO TO 200
  160 NI=MN+1
      NJ=MN
  200 PMN=P(N)
      DPMN=DP(N)
      PMMN=PM(N)
      SPH=SPHANK(N)
      FN=FLOAT(N*(N-1))
      CON=KRSQ*SPMUL
      SICO=CON*SINTH
      HI=CON*SPH
      HJ1=SICO*SPH
```

?

```
      HJ2=(RD*DPMN)*HJ1
      WH=WRK0*SPH
      WHD=WH+DSPHANK(N)
      HK1=SICO*WHD
      HK2=(RD*PMN*FN*SICO)*WH
      HL1=CON*WHD
      CON=CON*RD*PMN
      HL2=(CON*FN)*WH
      HL3=CON*WHD
      DO 300 MCOL=1,NHALF
      IF(M .EQ. 1) GO TO 250
      PIJ=P(NI)
      DPIJ=DP(NI)
      BESIJ=SPB(NI)
      CON=PMN*DPIJ+DPMN*PIJ
      DIJ=CON*BESIJ
      TDIJ=REAL(HI)*DIJ
      DIJ=HI*DIJ
      IMN1(MROW,MCOL)=IMN1(MROW,MCOL)+DIJ
      IMN2(MROW,MCOL)=IMN2(MROW,MCOL)+TDIJ
      WH=BESIJ*WRK1
      WHD=WH+DSPB(NI)
      SPH=CON*WHD
      DSPH=PIJ*WHD
      WTEM=(PIJ*FLOAT(NI*(NI-1)))*WH
      DIJ=SPH*HL1+DSPH*HL2+WTEM*HL3
      TDIJ=REAL(HL1)*SPH+REAL(HL2)*DSPH+REAL(HL3)*WTEM
      LMN1(MROW,MCOL)=LMN1(MROW,MCOL)+DIJ
      LMN2(MROW,MCOL)=LMN2(MROW,MCOL)+TDIJ
  250 PIJ=P(NJ)
      DPIJ=DP(NJ)
      PMIJ=PM(NJ)
      BESIJ=SPB(NJ)
      CON=PMMN*PMIJ+DPMN*DPIJ
      WH=BESIJ*WRK1
      WHD=WH+DSPB(NJ)
      SPH=CON*WHD
      DSPH=(FLOAT(NJ*(NJ-1))*PIJ)*WH
      DIJ=HJ1*SPH+HJ2*DSPH
      TDIJ=REAL(HJ1)*SPH+REAL(HJ2)*DSPH
      JMN1(MROW,MCOL)=JMN1(MROW,MCOL)+DIJ
      JMN2(MROW,MCOL)=JMN2(MROW,MCOL)+TDIJ
      SPH=CON*BESIJ
      DSPH=DPIJ*BESIJ
      DIJ=HK1*SPH+HK2*DSPH
      TDIJ=REAL(HK1)*SPH+REAL(HK2)*DSPH
      KMN1(MROW,MCOL)=KMN1(MROW,MCOL)+DIJ
      KMN2(MROW,MCOL)=KMN2(MROW,MCOL)+TDIJ
      NI=NI+2
      NJ=NJ+2
```

```
  300 CONTINUE
      N=N+1
      IFLAG=-IFLAG
  350 CONTINUE
      THETA=THETA+DTH
      COSTH=COS(THETA)
      SINTH=SIN(THETA)
  400 CONTINUE
  450 CONTINUE
      IF(M .EQ.1 ) GO TO 462
      WH=CMPLX(0.,FLOAT(M-1))
      DO 460 MCOL=1,NHALF
      DO 460 MROW=1,NMAX
      IMN1(MROW,MCOL)=WH*IMN1(MROW,MCOL)
      IMN2(MROW,MCOL)=WH*IMN2(MROW,MCOL)
      LMN1(MROW,MCOL)=WH*LMN1(MROW,MCOL)
      LMN2(MROW,MCOL)=WH*LMN2(MROW,MCOL)
  460 CONTINUE
  462 DO 465 MCOL=1,NHALF
      DO 465 MROW=1,NMAX
      KMN1(MROW,MCOL)=-KMN1(MROW,MCOL)
      KMN2(MROW,MCOL)=-KMN2(MROW,MCOL)
  465 CONTINUE
      IF(M .NE. 1) GO TO 464
      DO 466 MCOL=1,NHALF
      DO 466 MROW=1,NMAX
      WH=KMN1(MROW,MCOL)
      KMN1(MROW,MCOL)=JMN1(MROW,MCOL)
      JMN1(MROW,MCOL)=WH
      WH=KMN2(MROW,MCOL)
      KMN2(MROW,MCOL)=JMN2(MROW,MCOL)
      JMN2(MROW,MCOL)=WH
  466 CONTINUE
  464 IF(KEY .NE. 1) GO TO 475
      WRITE 3500,((IMN1(I,J),J=1,NHALF),I=1,NMAX)
      WRITE 3500,((JMN1(I,J),J=1,NHALF),I=1,NMAX)
      WRITE 3500,((KMN1(I,J),J=1,NHALF),I=1,NMAX)
      WRITE 3500,((LMN1(I,J),J=1,NHALF),I=1,NMAX)
      WRITE 3500,((IMN2(I,J),J=1,NHALF),I=1,NMAX)
      WRITE 3500,((JMN2(I,J),J=1,NHALF),I=1,NMAX)
 3500 FORMAT(///,(2X,8E13.6))
  475 IF(M .EQ.1) GO TO 477
      I=0
      DO 470 MCOL=1,NMAX,2
      I=I+1
      DO 470 MROW=1,NMAX,2
      PMTRX1(MROW,MCOL+1)=LMN1(MROW,I)+RATIO*IMN1(MROW,I)
      QMTRX1(MROW,MCOL+1)=IMN1(MROW,I)+RATIO*LMN1(MROW,I)
      PMTRX2(MROW,MCOL+1)=LMN2(MROW,I)+RATIO*IMN2(MROW,I)
      QMTRX2(MROW,MCOL+1)=IMN2(MROW,I)+RATIO*LMN2(MROW,I)
```

?

```
      PMTRX1(MROW+1,MCOL)=IMN1(MROW+1,I)+RATIO*LMN1(MROW+1,I)
      QMTRX1(MROW+1,MCOL)=LMN1(MROW+1,I)+RATIO*IMN1(MROW+1,I)
      PMTRX2(MROW+1,MCOL)=IMN2(MROW+1,I)+RATIO*LMN2(MROW+1,I)
      QMTRX2(MROW+1,MCOL)=LMN2(MROW+1,I)+RATIO*IMN2(MROW+1,I)
  470 CONTINUE
  477 I=0
      DO 480 MCOL=1,NMAX,2
      I=I+1
      DO 480 MROW=1,NMAX,2
      PMTRX1(MROW,MCOL)=KMN1(MROW,I)+RATIO*JMN1(MROW,I)
      QMTRX1(MROW,MCOL)=JMN1(MROW,I)+RATIO*KMN1(MROW,I)
      PMTRX2(MROW,MCOL)=KMN2(MROW,I)+RATIO*JMN2(MROW,I)
      QMTRX2(MROW,MCOL)=JMN2(MROW,I)+RATIO*KMN2(MROW,I)
      PMTRX1(MROW+1,MCOL+1)=JMN1(MROW+1,I)+RATIO*KMN1(MROW+1,I)
      QMTRX1(MROW+1,MCOL+1)=KMN1(MROW+1,I)+RATIO*JMN1(MROW+1,I)
      PMTRX2(MROW+1,MCOL+1)=JMN2(MROW+1,I)+RATIO*KMN2(MROW+1,I)
      QMTRX2(MROW+1,MCOL+1)=KMN2(MROW+1,I)+RATIO*JMN2(MROW+1,I)
  480 CONTINUE
C
C
C   ***  DECOMPOSE THE MATRIX ****
C
C
      CALL LEQT2C(PMTRX1,NMAX,20,Y,1,20,1,WA1,IER)
      IF(IER .EQ. 129) GO TO 760
      CALL LEQT2C(QMTRX1,NMAX,20,Y,1,20,1,WA2,IER)
      IF(IER .EQ. 129) GO TO 760
      DO 600 I=1,KMAX
      IF(I .NE. 1) GO TO 500
      IF(M .NE. 2) GO TO 600
  500 CALL LEGENDR(COA(I),SIA(I),M,MN,NMAX)
      SPH=-(IMG**MN)
      K=MN
      IF(M .EQ. 1) GO TO 510
      DO 505 J=1,NMAX,2
      COEF1(J)=PM(K)*SPH
      COEF2(J)=DP(K)*SPH
      SPH=SPH*IMG
      K=K+1
      COEF1(J+1)=DP(K)*SPH
      COEF2(J+1)=PM(K)*SPH
      SPH=SPH*IMG
      K=K+1
  505 CONTINUE
      GO TO 520
  510 DO 515 J=1,NMAX,2
      COEF1(J)=DP(K)*SPH
      COEF2(J)=PM(K)*SPH
      SPH=SPH*IMG
      K=K+1
?
```

```
      COEF1(J+1)=PM(K)*SPH
      COEF2(J+1)=DP(K)*SPH
      SPH=SPH*IMG
      K=K+1
  515 CONTINUE
  520 IPQ=0
  525 IPQ=IPQ+1
      IPOL=(IPQ+1)/2
      GO TO (530,540,550,560,600) IPQ
  530 DO 535 J=1,NMAX
      Y(J)=COEF1(J)
  535 CONTINUE
      GO TO 580
  540 IF(I .EQ. KMAX) GO TO 525
      DO 545 J=1,NMAX
      Y(J)=COEF2(J)
  545 CONTINUE
      GO TO 570
  550 IF(I .EQ. KMAX) GO TO 525
      IF(I .EQ.1) GO TO 600
      DO 555 J=1,NMAX
      Y(J)=IMS*COEF2(J)
  555 CONTINUE
      GO TO 580
  560 DO 565 J=1,NMAX
      Y(J)=IMS*COEF1(J)
  565 CONTINUE
  570 CALL LEQT2C(QMTRX1,NMAX,20,Y,1,20,2,WA2,IER)
      WRITE 2250,(Y(J),J=1,NMAX)
 2250 FORMAT(//,(4X,8E13.6))
      IF(IER .EQ. 130) GO TO 770
      CALL MULTRX(QMTRX2,X,Y,20,NMAX)
      GO TO 590
  580 CALL LEQT2C(PMTRX1,NMAX,20,Y,1,20,2,WA1,IER)
      WRITE 2250,(Y(J),J=1,NMAX)
      IF(IER .EQ. 130)GO TO 770
      CALL MULTRX(PMTRX2,X,Y,20,NMAX)
  590 WRITE 2200, M,IPOL,(I-1)*DAL,(X(J),J=1,NMAX)
 2200 FORMAT(///,2X,*M=*,I2,2X,*POL*,I2,2X,*INCIDENCE ANGLE*,F7.2,//,
     1          (2X,8E15.8))
      CALL SCATTER(M,MN,NMAX,IPOL,IPQ,SCAT,TOT)
      IF(A .EQ. B .AND. IPQ .EQ.1) CALL SPHERE(M,MN,NMAX,EPS,RK0,RK1)
      IF(M .NE. 1) GO TO 595
      SCAT=0.5*SCAT
      TOT=0.5*TOT
  595 QS(I,IPOL)=QS(I,IPOL)+SCAT
      QT(I,IPOL)=QT(I,IPOL)+TOT
      GO TO 525
  600 CONTINUE
  700 CONTINUE
?
```

```
      R0=8.*PI/(K0*K0)
      QT(1,2)=QT(1,1)
      QS(1,2)=QS(1,1)
      DO 750 I=1,KMAX
      DO 750 J=1,2
      QT(I,J)=QT(I,J)*R0
      QS(I,J)=QS(I,J)*R0
      QA(I,J)=QT(I,J)-QS(I,J)
  750 CONTINUE
      WRITE 2000, A,B,FREQ,EPS,KB,NMAX,MMAX,KMAX,NSECT
      WRITE 2500
 2500 FORMAT(///,40X,*CROSS SECTIONS*,//)
      WRITE 3600,((I-1)*DAL,(QA(I,J),J=1,2),(QS(I,J),J=1,2),
     1              (QT(I,J),J=1,2),I=1,KMAX)
 3600 FORMAT(2X,*INCIDENCE ANGLE*,10X,
     1        *ABSORPTION*,20X,*SCATTERING*,20X,*EXTINCTION*,///,
     2         (6X,F6.2,5X,6E15.7,/))
      R0=1./(PI*A)
      DO 755 I=1,KMAX
      R2=R0/SQRT(BSQ*SIA(I)**2+ASQ*COA(I)**2)
      DO 755 J=1,2
      QT(I,J)=QT(I,J)*R2
      QS(I,J)=QS(I,J)*R2
      QA(I,J)=QA(I,J)*R2
  755 CONTINUE
      WRITE 2550
 2550 FORMAT(///,40X,*EFFICIENCIES*,//)
      WRITE 3600 ,((I-1)*DAL,(QA(I,J),J=1,2),(QS(I,J),J=1,2),
     1             (QT(I,J),J=1,2),I=1,KMAX)
      GO TO 800
  760 WRITE 2600,M
 2600 FORMAT(2X,*M=*,I3,*  MATRIX IS SINGULAR*)
      GO TO 800
  770 WRITE 2700,M
 2700 FORMAT(2X,*M=*,I3,*  MATRIX IS ILL-CONDITIONED*)
  800 STOP
      END
JFM
```

```
      SUBROUTINE SCATTER(M,MN,NMAX,IPOL,IPQ,SCAT,TOT)
      COMPLEX X(20),SP,IMS,WASP
      REAL P(40),DP(40),PM(40)
      COMMON/BLK1/P,DP,PM/BLK4/X
      IMS=(0.,-1.)
      COM=1./FACT(M+M-1)
      F=0.
      L=MN-1
      FL=FLOAT(L)
      G=FL+FL
      SP=IMS**(L-IPOL)
      S=0.5
      IF(IPQ .EQ. 2 .OR. IPQ .EQ. 3) S=-0.5
      SCAT=0.
      WASP=(0.,0.)
      IF(M .EQ. 1) S=-S
    5 DO 10 I=1,NMAX
      L=L+1
      TEMP=(FL+FL+1.)*COM/(FL*(FL+1.))
      SCAT=SCAT+TEMP*CABS(X(I))**2
      TEMP=TEMP*(PM(L)*(S+0.5)+DP(L)*(0.5-S))
      WASP=WASP+TEMP*SP*X(I)
      S=-S
      SP=SP*IMS
      FL=FL+1.
      F=F+1.
      G=G+1.
      COM=COM*F/G
   10 CONTINUE
      TOT=REAL(WASP)
      RETURN
      END
?
```

```
      SUBROUTINE HANKEL(X,MN,N)
      COMPLEX SPHANK(40),DSPHANK(40)
      REAL SPB(70),SPN(40),DSPN(40)
      COMMON/BLK2/SPHANK,DSPHANK
      ETA=COS(X)
      STA=SIN(X)
      Y=1./X
      NL=MN+N
      SPN(1)=C1=-ETA*Y
      SPN(2)=C2=(C1-STA)*Y
      DSPN(1)=-C2
      D=1.
      S=0.
      DO 10 I=3,NL
      D=D+2.
      S=S+1.
      SPN(I)=C3=D*C2*Y-C1
      DSPN(I-1)=(S*C1-(S+1.)*C3)/D
      C1=C2
      C2=C3
   10 CONTINUE
      M=NL+30
      K=IFIX(ABS(X))
      IF(K .GT. NL) M=K+30
      C1=0.
      C2=1.
      D=FLOAT(M+M+1)
      J=M-1
      K=M
      DO 20 I=1,J
      D=D-2.
      K=K-1
      SPB(K)=C3=D*C2*Y-C1
      C1=C2
      C2=C3
   20 CONTINUE
      C1=STA*Y
      FACTOR=C1/C3
      SPHANK(1)=CMPLX(C1,SPN(1))
      C2=FACTOR*SPB(2)
      SPHANK(2)=CMPLX(C2,SPN(2))
      DSPHANK(1)=CMPLX(-C2,DSPN(1))
      F=1.
      DO 30 I=3,NL
      C3=SPB(I)*FACTOR
      SPHANK(I)=CMPLX(C3,SPN(I))
      DSPHANK(I-1)=CMPLX((F*(C1-C3)-C3)/(F+F+1.),DSPN(I-1))
      C1=C2
      C2=C3
      F=F+1.
   30 CONTINUE
      RETURN
      END
```

```
      SUBROUTINE SPHBESS(X,MN,N)
      COMPLEX X,Y,FACTOR,C1,C2,C3,SPB(100),DSPB(40)
      COMMON/BLK3/SPB,DSPB
      Y=(1.,0.)/X
      NL=N+MN
      M=NL+30
      IF(CABS(X) .GT. 10.) M=NL+50
      IF(M .GT. 100) M=100
      C1=(0.,0.)
      C2=(1.,1.)
      K=M
      F=FLOAT(M+M+1)
      M=M-1
      DO 50 I=1,M
      K=K-1
      F=F-2.
      SPB(K)=C3=F*C2*Y-C1
      C1=C2
      C2=C3
   50 CONTINUE
      SPB(1)=C1=CSIN(X)*Y
      FACTOR=C1/C2
      SPB(2)=C2=FACTOR*SPB(2)
      DSPB(1)=-C2
      F=1.
      DO 60 I=3,NL
      SPB(I)=C3=SPB(I)*FACTOR
      DSPB(I-1)=(F*(C1-C3)-C3)/(F+F+1.)
      C1=C2
      C2=C3
      F=F+1.
   60 CONTINUE
      RETURN
      END
?
```

```
      SUBROUTINE LEGENDR(ETA,ST,M,MN,N)
      REAL P(40),DP(40),PM(40)
      COMMON/BLK1/P,DP,PM
      NM=N+MN+1
      IF(ETA .EQ. 1.) GO TO 40
      F=FLOAT(M)
      CM=FLOAT(M+M-1)
      X=ST**(M-1)
      SM=(F-1.)/ST
      P(M)=PA1=X*DFACT(M-1)
      P(M+1)=PA2=ETA*PA1*CM
      DP(M)=(PA2-F*ETA*PA1)/ST
      PM(M)=SM*PA1
      PM(M+1)=SM*PA2
      CM=CM-2.
      F=F-1.
      DO 20 I=2,NM
      FI=FLOAT(I)
      TEMP=ETA*PA2
      P(I+M)=PA3=TEMP+TEMP-PA1+CM*(TEMP-PA1)/FI
      DP(I+M-1)=(FI*PA3-(F+FI)*TEMP)/ST
      PM(I+M)=SM*PA3
      PA1=PA2
      PA2=PA3
   20 CONTINUE
      RETURN
   40 IF(M .EQ. 2) GO TO 60
      FI=0.
      IF(M .EQ. 1) FI=1.
      DO 50 I=M,NM
      P(I)=FI
      DP(I)=0.
      PM(I)=0.
   50 CONTINUE
      RETURN
   60 DO 100 I=M,NM
      P(I)=0.
      F=FLOAT(I)
      F=0.5*F*(F-1.)
      DP(I)=F
      PM(I)=F
  100 CONTINUE
      RETURN
      END
?
```

```
      SUBROUTINE SPHERE(M,MN,NMAX,EPS,RK0,RK1)
      REAL P(40),DP(40),PM(40)
      COMPLEX RK1,B1,WBD,SP,SM,R1,WR1,FAC,WA,WB,EPS
      COMPLEX SPHANK(40),DSPHANK(40),SPB(100),DSPB(40)
      COMMON/BLK1/P,DP,PM/BLK2/SPHANK,DSPHANK/BLK3/SPB,DSPB
      WRITE 500,M
  500 FORMAT(//,2X,*EXACT SOLUTION FOR THE SPHERE,  M=*,I3,/)
      DO 100 I=MN,NMAX
      B1=SPB(I)
      WBD=DSPB(I)
      SP=SPHANK(I)
      SM=DSPHANK(I)
      A1=REAL(SP)
      WAD=REAL(SM)
      R1=RK0*WAD+A1
      WR1=RK1*WBD+B1
      FAC=RK0*SM+SP
      WA=PM(I)*(B1*R1-A1*WR1)/(B1*FAC-SP*WR1)
      WB=DP(I)*(A1*WR1-EPS*B1*R1)/(SP*WR1-EPS*B1*FAC)
      WRITE 600,WA,WB
  600 FORMAT(5X,4E20.12)
  100 CONTINUE
      RETURN
      END
?
```

```
      SUBROUTINE MULTRX(A,X,Y,M,N)
      COMPLEX A(M,M),X(M),Y(M),SUM
      DO 20 I=1,N
      SUM=(0.,0.)
      DO 10 J=1,N
      SUM=SUM+A(I,J)*Y(J)
   10 CONTINUE
      X(I)=SUM
   20 CONTINUE
      RETURN
      END
?
```

```
      SUBROUTINE SHAPE(ETA,ZETA,RKØ,RK1,RD,WRKØ,WRK1,KRSQ)
      REAL KØ,KRSQ
      COMPLEX K1,WRK1,RK1
      COMMON/BLKS/ASQ,BSQ,AB,ABQ,KØ,K1
      FACTOR=ASQ*ETA*ETA+BSQ*ZETA*ZETA
      R=AB/SQRT(FACTOR)
      RKØ=R*KØ
      RK1=R*K1
      WRKØ=1./RKØ
      WRK1=(1.,Ø.)/RK1
      KRSQ=RKØ*RKØ
      RD=ABQ*ETA*ZETA/FACTOR
      RETURN
      END



      FUNCTION DFACT(N)
      DFACT=1.
      IF( N .EQ. Ø) RETURN
      DO 1Ø I=1,N
      DFACT=DFACT*FLOAT(I+I-1)
   1Ø CONTINUE
      RETURN
      END



      FUNCTION FACT(N)
      FACT=1.
      IF(N .EQ. 1) RETURN
      DO 1Ø I=2,N
      FACT=FACT*FLOAT(I-1)
   1Ø CONTINUE
      RETURN
      END
```

-END OF FILE-

?

TECHNICAL REPORT DATA
(Please read Instructions on the reverse before completing)

1. REPORT NO. EPA-600/1-79-025	2.	3. RECIPIENT'S ACCESSION NO.
4. TITLE AND SUBTITLE Absorption Characteristics of Prolate Spheroidal Model of Man and Animals At and Near Resonance Frequency		5. REPORT DATE August 1979
		6. PERFORMING ORGANIZATION CODE
7. AUTHOR(S) V.K. Tripathi and H. Lee		8. PERFORMING ORGANIZATION REPORT NO.
9. PERFORMING ORGANIZATION NAME AND ADDRESS Electrical and Computer Engineering Department, Oregon State University, Corvallis, Oregon 97331		10. PROGRAM ELEMENT NO. 1FA628
		11. CONTRACT/GRANT NO. R-804697-01-1
12. SPONSORING AGENCY NAME AND ADDRESS Health Effects Research Laboratory, Office of Research and Development, US Environmental Protection Agency, Research Triangle Park, NC 27711	RTP, NC	13. TYPE OF REPORT AND PERIOD COVERED Final, 9-15-76 to 3-15-78
		14. SPONSORING AGENCY CODE EPA 600/11
15. SUPPLEMENTARY NOTES		

16. ABSTRACT

This report deals with the evaluation of the absorption characteristics of prolate spheroidal models of man and animals consisting of homogeneous biological tissues irradiated with plane waves at an arbitrary angle of incidence at and near the resonance frequency. Stevenson's series expansion method in the third approximation and the extended boundary condition method are presented in detail since they were found to be most amenable to the solution of the problem.

A general formulation of Stevenson's method in the third approximation is presented which can be applied to an arbitrary angle of incidence and leads to an improvement in frequency range of validity and accuracy as compared with first order solutions.

The report also deals in detail with the extended boundary condition method (EBCM), since it was found to be inplementable for realistic models at frequencies approaching resonance. Though the EBCM theory is well known, the application of the method has been stressed and certain improvements in the accuracy and efficiency of the computations are incorporated. Numerical results are presented and compared with known data published by others.

17. KEY WORDS AND DOCUMENT ANALYSIS

a. DESCRIPTORS	b. IDENTIFIERS/OPEN ENDED TERMS	c. COSATI Field/Group
Electromagnetic radiation, radio frequency, microwaves, electromagnetic absorption, resonance, numerical methods, mathematical models, spheres, muscle tissue, humans, laboratory animals, standards, protection.		06F

18. DISTRIBUTION STATEMENT Release to Public	19. SECURITY CLASS (This Report) Unclassified	21. NO. OF PAGES 71
	20. SECURITY CLASS (This page) Unclassified	22. PRICE

EPA Form 2220-1 (Rev. 4-77) PREVIOUS EDITION IS OBSOLETE